8-2009

The implementation and analysis of through wall radar systems

Xiaohui Wang
University of Texas-Pan American

THE IMPLEMENTATION AND ANALYSIS OF THROUGH WALL RADAR SYSTEMS

A Thesis

By

XIAOHUI WANG

Submitted to the Graduate School of the
University of Texas Pan-American
In partial Fulfillment of the requirements for the Degree of

MASTER OF SCIENCE

August 2009

Major Subject: Electrical Engineering

ABSTRACT

Xiaohui Wang, The Implementation and Analysis of Through-Wall Radar Systems. Master of Science (MS), August 2009, 61 pp.; 66 figures, references, 24 titles.

Through wall radar detecting, locating, imaging and tracking is a topic of current research interest in connection with law enforcement, urban area operations and search and rescue missions. Up to now, three different radar techniques are employed in through wall radar systems, including impulse through wall radar, continuous wave radar and swept frequency radar. In this thesis, we set out to give a comparison of these three kinds of through wall radar systems. First,we studied the challenges caused by the wall in through wall radar systems. Second,we implemented these three kinds of through wall radar system. In each kind of through wall radar, we developed Labview codes to realize automatic measurement and data acquisition, then we processed the data by different algorithms, including elliptic curve imaging method, Doppler-DOA method. Finally we analyzed the performance of each kind of radar system, compared the advantages and disadvantages to given a guide of through wall radar design.

ACKNOWLEDGEMENT

First, I would like to give my thanks to my supervisor, Dr.Junfei Li for his excellent guide during my study in USA. His research idea, advice, valuable lesson during two years of study give me a significant contribution regarding this thesis. More over, his positive research attitude give me an endure influent for my career in the future. I appreciate all he has done for me.

Second, I want to give my great thanks to Dr. Heinrich Foltz and Dr.Zhijun Qiao, for willing to serve on my thesis committee, taking time to read my thesis and give me wonderful comments for the revision.

Big thanks will also go to Dr. Jiadong Xu, my former supervisor in Northwestern Polytechnical University, who leads me to the fields of electromagnetic area and gave me a recommendation to study abroad. I would say his support changes my life and career.

I also want to give my thanks to Jing Wang and Polash, who helped me a lot when I first came to USA. They also taught me a lot and made me adapt the life in UTPA quickly.

Special thanks will give to the CSSA-RGV members and Chinese friend in the church. They really helped me a lot in my life and gave me lots of good memory.

The final thanks belong to my parents and my family, for their unconditional love and support.

TABLE OF CONTENT

LIST OF FIGURES

LIST OF TABLES

CHAPTER 1

INTRODUCTION

1.1 Background of through-wall radar

A through wall radar is a radar system that tries to get the target information through the most common building materials including reinforced concrete, concrete block, cinder block, sheet rock, brick, wood, plastic, tile, etc. Recently, through-wall radar system is a popular research area due to its large range of applications in both military and civilian areas. It includes through wall radar detection, static target location, imaging and moving target tracking. Fig1.1 shows an example of through wall radar application in hostage rescue.

Fig1.1 Through-wall radar detection in hostage rescue scenario [1]

Recent advances in RF design and digital signal processing have accelerated the development of through-wall radar systems with numerous security related applications.

- Search and Rescue

Through wall radar can be designed to have high sensitivity to very small movements, such as human breathing and heart rate, so it can be used in detection of people through collapsed building debris and rubble.

- Hostage rescue

Through wall radar can be used to determine whether rooms are occupied before entry and give high reliability of detection, so police can know where hostages are congregated or soldiers can tell where the enemy is lying. This reduces the risks significantly for the police to rescue the hostage successfully.

- Area surveillance and tracking

Through wall surveillance is a difficult but important problem for both law enforcement and military personnel. It can be used in traffic monitoring, pedestrian crossing monitoring automotive safety systems, through wall imaging during fire.

1.2 Current Research

The broad use of through wall radar inspires the research in this area. The recent advance in RF design and digital signal processing has especially accelerated the development of through wall radar detection and imaging.

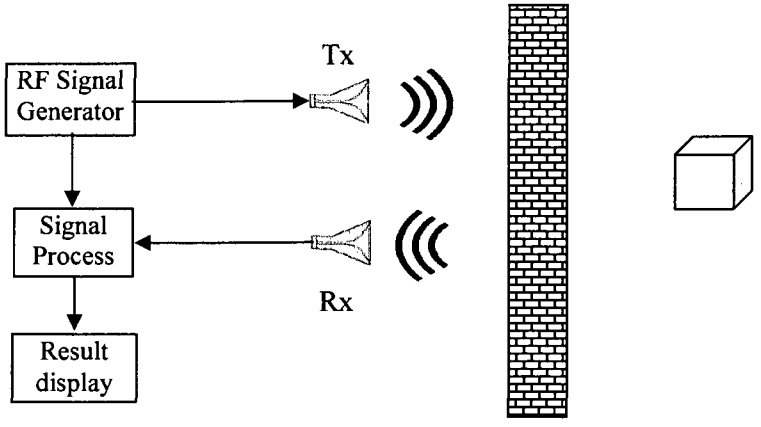

Fig1.2 The block diagram of through radar

The working principle of through wall radar system is illustrated in Fig1.2. The signal source sends the RF signal to the transmitter antenna. After the electromagnetic wave propagates through the wall, it hits the targets under detection and then bounces back. The receiver antenna receives the echoed signal which contains the information of the target in the other side of the wall. The detection result can be achieved from different algorithms.

1.2.1 The influence of the wall

The characteristic of the wall plays a critical role because through wall radar detection and imaging requires wave penetrating through the specific building materials such as concrete blocks, clay bricks, drywall, asphalt shingles, fiberglass insulation, plywood etc. the influence of the wall includes three aspects- electromagnetic power loss, direction change in wave propagation and phase distortion.

Power loss

The power loss of the wall is an important issue due to the signal noise ratio (SNR) requirement in target detection. In the through wall radar, the power loss includes several parts: the free space loss, reflection from air-wall interface and loss in the wall. The propagation loss inside the wall may be significant if the wall has large permittivity and thickness.

A lot of work has been devoted to the research on the wall characteristics [3][5]. Lawrence Frazier measured the one way insertion loss of different materials in frequency domain [3]. Fig1.3 shows the one way loss of different materials, more detail regarding the loss of concrete is shown in Fig1.4 (a). Fig1.4 (b) also shows the one way loss of lumber with different thickness measured by the author.

From Fig1.3 and Fig1.4 we can see that the electromagnetic waves can penetrate through the concrete wall without massive attenuation up to approximately 3-4 GHz, but it can penetrate the lumber wall without massive loss up to 12 GHz.

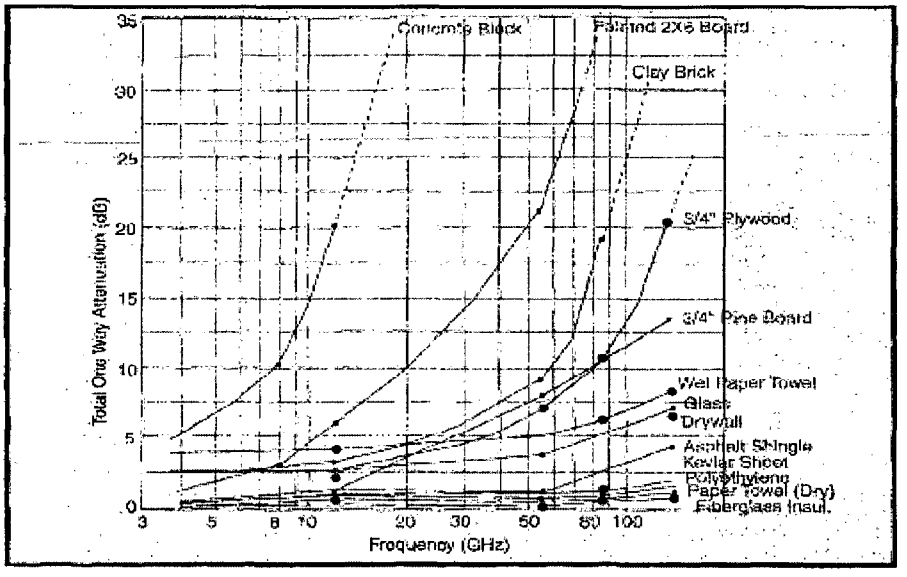

Fig1.3 One way loss measurement of different materials [3]

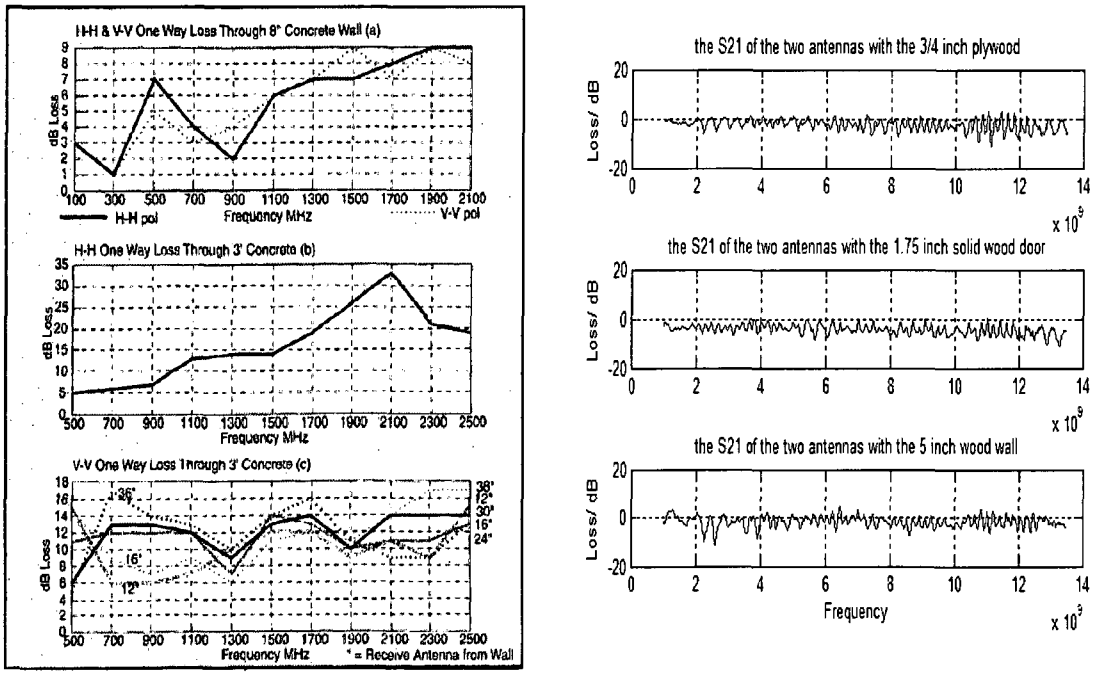

(a) The insertion loss of concrete [3] (b) the insertion loss of lumber

Fig1.4 The one way insertion loss of concrete and lumber material

Change in direction-Snell's law

When the wave arrives to the wall at a certain angle, the wave in the air will continue its propagation but with changed direction. This holds in the case when the permittivity of the wall differs from the permittivity of the layer in front of the wall. Even more, when the wave is leaving the wall, it changes its direction once more. When the permittivity of the wall is greater than the permittivity in the air, the wave velocity in the wall will be lower than that in the free space. The velocity in the wall is given by:

$$v_W = \frac{c}{\sqrt{\varepsilon_{rW}}} \tag{1.1}$$

Where, ε_{rW} is the permittivity of the wall.

When the microwave passes through an interface between two materials with different permittivity at an oblique angle, both reflected and refracted wave are produced. The relationship between incidence angle and refraction angle is given by the Snell's law.

$$\frac{\sin\theta_1}{\sin\theta_2} = \frac{v_1}{v_2} \tag{1.2}$$

Where, θ_1 is the incidence angle and θ_2 is the refraction angle, v_1 and v_2 are the microwave propagation velocity in medium 1 and medium2.

Fig1.5 shows the microwave propagation from air through wall. According to equation (1) and equation (2), the incidence angle and the refraction angle inside the wall is given:

$$\frac{\sin\theta_1}{\sin\theta_2} = \sqrt{\frac{\varepsilon_W}{\varepsilon_A}} \tag{1.3}$$

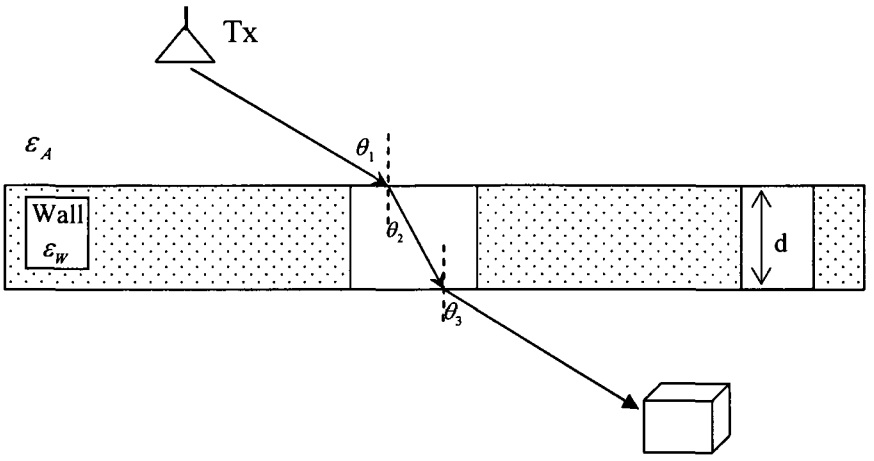

Fig1.5 The wave propagation path in through homogenous wall scenario

An interesting thing is that the incident angle θ_1 before the wall and the second refraction angle θ_3 are the same if the material of the wall is homogenous. The different wave propagation velocity in the wall and refraction will make the time and range estimation more complicated.

Phase distortion

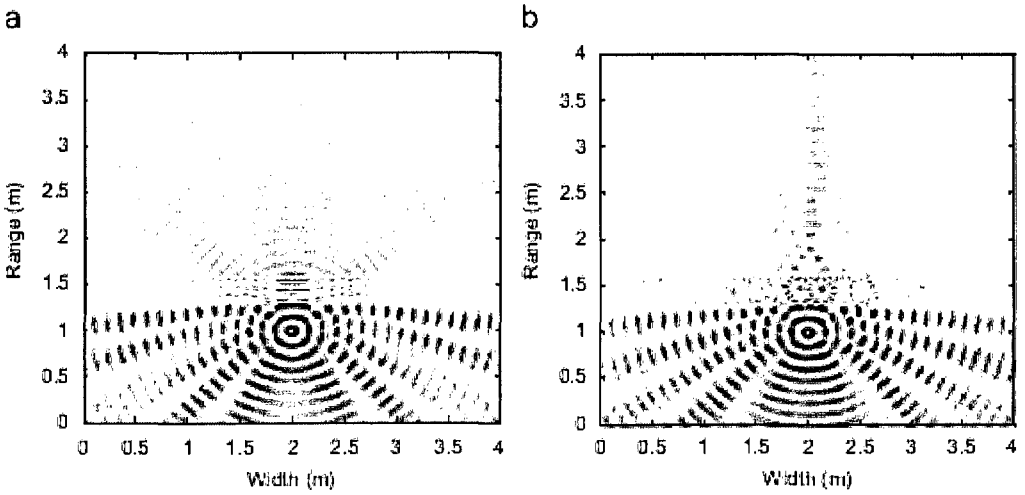

Fig1.6 FDTD simulation result of wall propagation (a) a solid homogenous wall and (b) an inhomogeneous cinder block wall [4]

When the microwave propagates through the wall, not only will the amplitude be attenuated, but also the phase distortion will occur. To illustrate the microwave

transmission physics, a two-dimensional FDTD simulation was carried out on both a solid homogeneous wall and a cinder block wall structure with air holds [4]. The thicknesses of both walls are 30cm, with relative permittivity of the concrete set at 5. A 2.4 GHz sinusoidal source is used and the distance between the source and the wall is also 30cm in both cases. As can be seen in the sinusoidal steady-state field plots of Fig1.6, the wave front transmitted through the solid homogeneous wall remains a well behaved spherical front, while the transmitted wave through the inhomogeneous cinder block wall shows considerable reverberation near the wall [4]. The simulations also indicated that at a sufficiently far distance from the wall, the wave front begins to resemble the regular spherical spread.

In essence, the cinder block structure acts like an array that re-radiates the impinging wave front. Therefore, in the near field of the array, the transmitted field is quite complex. When the sufficient distance is reached, the wave front approaches that of the far field. The actual far-field distance depends on the illuminated aperture of the wall from the primary source [4].

1.2.2 Source waveforms of through-wall radar

- Impulse

Since the penetration loss of the wall is a function of frequency, we have to choose the signal source with certain frequency components to penetrate the wall. As discussed in the latest section, the signal with low frequency component has better penetration while the high frequency component has larger insertion loss.

An ultra-wide band pulse is a commonly used candidate due to its better penetration ability and high range resolution. In the ultra wide band pulse radar system,

pulse selection plays an important part in the high imaging resolution [10]. The typical pulse is a Gaussian pulse given by

$$p(t) = (\sqrt{2}/\alpha)\exp(-2\pi t^2/\alpha^2) \tag{1.4}$$

Where, $\alpha^2 = 4\pi\sigma^2$, σ is variance of the Gaussian signal, for the derivation action of the antenna, the transmit signal s(t) is a first derivative Gaussian pulse:

$$dp(t)/dt = t\exp(-2\pi t^2/\alpha^2) \tag{1.5}$$

And the received signal r(t) of Rx is a second derivative Gaussian pulse, which is the derivation of s(t) expressed as:

$$d^2p(t)/dt^2 = (1-4\pi t^2/\alpha^2)\exp(-2\pi t^2/\alpha^2) \tag{1.6}$$

The basic shape of the first and second derivative Gaussian pulse are plotted in Fig1.7

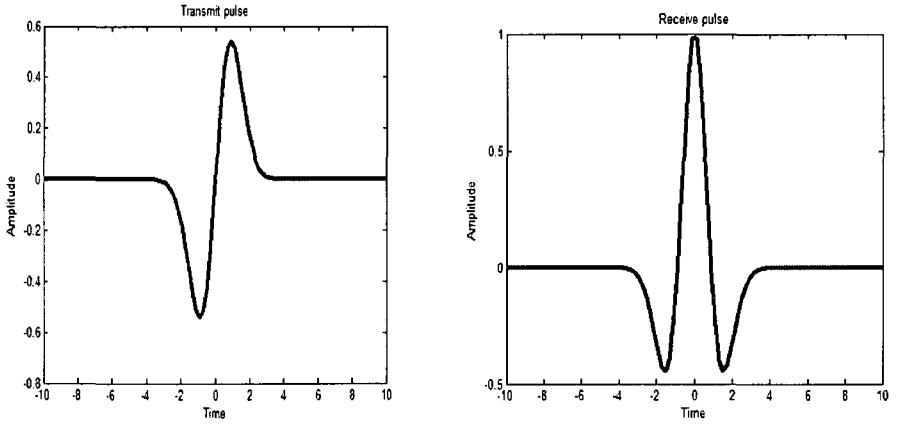

(a) Transmit pulse (b) Receive pulse

Fig1.7 Typical Gaussian pulses [10]

The spectrum of impulse and the through wall propagation are studied by W.A van, Cappellen and Radim[6]. It shows that the short pulse generated by pulse generator (K2-63-2) has a 50% width of 85 picoseconds and a bandwidth of about 5GHz.

- Linear frequency modulated wave

Linear frequency modulated signal (LFM) is usually called linear chirp signal. It is commonly used in radar system. In a linear chirp, the instantaneous frequency varies linearly with the time:

$$f(t) = f_0 + \alpha t \tag{1.7}$$

Where f_0 is the starting frequency, α is the rate of the frequency increase or chirp rate. The corresponding time domain function for a sinusoidal linear frequency modulated signal is:,.

$$s(t) = \sin(2\pi(f_0 t + \frac{1}{2}\alpha t^2)) \tag{1.8}$$

Fig1.8 shows the waveform in time domain of a chirp signal with $f_0 = 0$ and $\alpha = 100$.

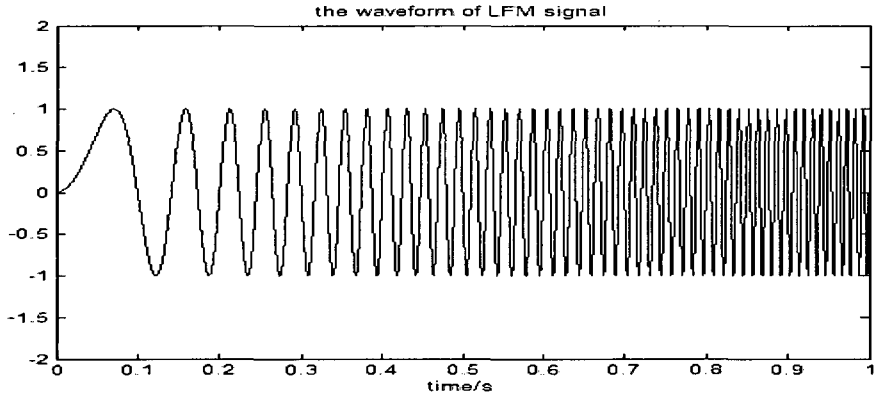

Fig1.8 The waveform of a linear modulated signal

- Continuous Wave

The continuous wave radar has the prominent advantage to detect the moving target by Doppler. In addition, it also can have better penetration as long as the frequency is suitable. Lots of research has been done regarding CW through radar detection.

Shobha Sundar Ram and H. Ling have studied the Doppler-based detection and tracking of human in indoor environments [4]. The micro-Doppler characteristics of

humans are detected by CW radar. The azimuth and elevation are also derived using a simple antenna array. Although it is hard to gather the range information with single frequency, by employing frequency diversity, the CW radar can also track the range of the moving targets.

1.3 Different algorithms of through radar detection and imaging

1.3.1 Elliptic Curve Intersection

The elliptic curve intersection method is the most conventional method to location the target in the through-wall radar system. Assume the microwave propagation distance between the transmitter, target and receiver is known, then the target under detection should located on the elliptic curve with two focies Tx, Rx whose major axis length is the propagation distance. By employing a receiver array, more than two elliptic curves can be generated. The target location can be focused at the intersection.

The propagation distance between transmitter, target and receiver is usually calculated by the time of arrive (TOA) [12]. However it will cause errors in the real application due to the wall effect, because the microwave propagation velocity in the wall is different from the velocity in the air. More over, the propagation route is also changed due to the refraction. So Lin and Zhang developed the virtual elliptic curve imaging method [10] based on solving the simultaneous equations of incident angle and refraction angle of both microwave forward traveling path and backward traveling path.

1.3.2 Doppler detection

Shobha Ram and Ling did a lot of work [4] on the continuous-wave Doppler radar detection. Compared to other radar system and algorithm, the CW radar has the advantage to suppress the stationary clutter.

The CW radar uses the phase different of the scattered signal at the two elements to determine the direction of arrival (DOA) of the target. The short time Fourier transform is used to get the spectrogram of the received signal. By employing an antenna array in horizontal direction or elevation direction, both the azimuth angle and elevation angle can be detected. More over, if frequency diversity is introduced to the CW Doppler radar system, the range information of the target could be estimated. In addition, Doppler discrimination facilitates the tracking of multiple movers due to their different moving velocities.

Although in the Doppler and DOA domain we can discriminate different targets with different Doppler, sometimes it happens that the Doppler of different target overlap. By combining Doppler processing with spatial beam forming in a multi-element array, it becomes possible to resolve targets along two dimensions, Doppler and DOA [4].

1.3.3 SAR imaging

SAR is the abbreviation of "Synthetic Aperture Radar", which has wide applications in remote sensing and imaging. SAR imaging can be achieved by moving a single antenna to illuminate the target region. There are several migration algorithms which can be used to image the object behind the wall [24]. In order to transform time domain in to the depth domain, where the depth means the direction from antenna to the target, the simple 2-D SAR imaging in time domain can be used. It is a migration with simple geometrical approach often called back projection or diffraction summation [24].

1.4 Research objective and thesis contribution

As we discussed in Section1.1, 1.2 and 1.3, the through wall radar has very large range of applications. Different applications impose different requirements on the

through wall radar. In the hostage rescue application, it requires that the through wall radar has reliable location of people, good resolution to identify the number of people and clear radar imaging to see inside condition of the room. But in the searching and rescue application, for instance, we need to search if there are any people under the collapse building after the earthquake, it requires the through wall radar to have high sensitivity to very small movements from human breathing and heart rate.

Since different applications have different requirements and different through wall radar implementations of have different characteristics, it is necessary to have a study and comparison of different kinds of through wall radar.

In this thesis, we implement three kinds of through-wall radar systems: impulse radar, swept frequency and radar CW radar in the following chapter2, 3 and4. In each section of the through wall radar, the automatic data collecting software is developed by Labview. The data then is processed to get the final result.

In chapter 5, the characteristics of three different through-wall radar systems are compared, the advantages and disadvantages are shown to give a basic guide to develop the through wall radar.

CHAPTER 2

IMPULSE THROUGH-WALL RADAR SYSTEM

In this section, first we use impulse radar to detect and locate the target behind a plywood board. Second the elliptic curve intersection method is introduced to form the image of the stationary targets.

2.1 Characteristics of impulse radar

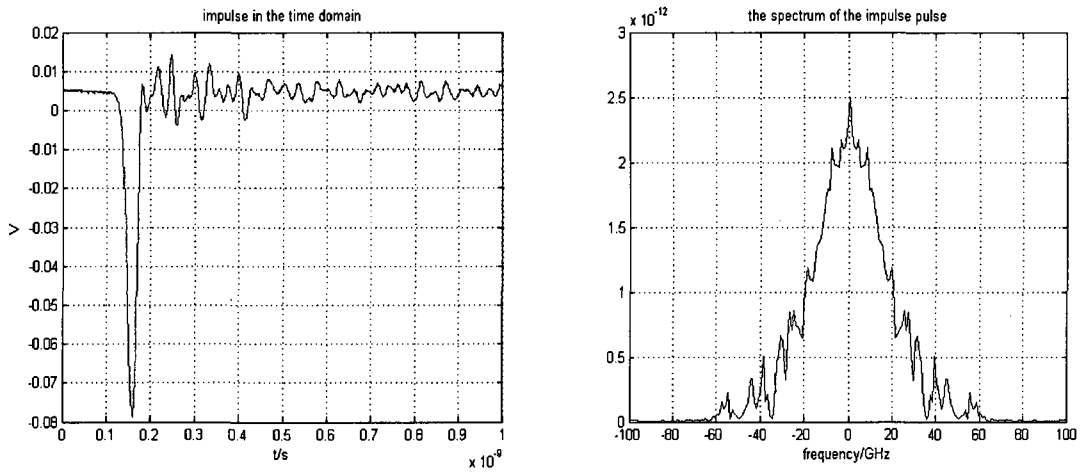

(a) The transmitting signal in time domain (b) the spectrum of the impulse

Fig2.1The impulse transmitting signal

The short pulse radar has some apparently advantages comparing to the conventional radar.

- The short pulse radar has a high range resolution. As we know the range resolution is $c\tau/2$, where τ is the pulse duration time, we can get a very high range resolution.
- Better penetration due to the richness of low frequency components. The higher frequency, the more attenuation it will have, especially in the lossy media

- High power efficiency because of low transmits duty cycle. This makes it difficult for surveillance subjects to know that they are being monitored.

The pulse generator 4015D from Picosecond Pulse Labs provides us a short pulse with about 66ps duration. Figure 2.1 shows the impulse in both time domain and frequency domain. From Fig2.1 (b), we can see that the short pulse has a bandwidth about 20GHz.

2.2 Hardware configuration

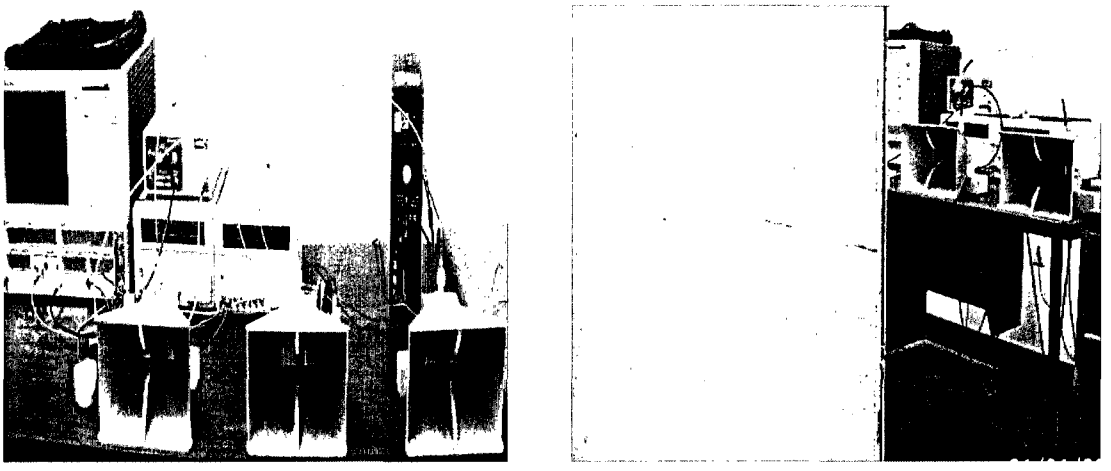

(a) The hardware connection (b) the 3/4"plywood wall

Fig2.2 The hardware configuration of impulse radar system

Fig2.2 shows the hardware configuration and connection of the impulse radar. The trigger output of the pulse generator 4015D is connected to the external trigger of the TDS8200 to have time coherence, while the driver output of the pulse generator was sent to the transmitter-double ridged horn antenna. The HRN-0118 has a frequency band from 1GHz to 18 GHz, which matches the spectrum of the short pulse. Figure2.3 shows the gain of HRN-0118 as a function of frequency.

The impulse response of the target was first received by the receiver antenna array under the control of the microwave switch, then passed through a microwave signal amplifier, and finally was sent the signal to the digital sampling oscilloscope Tektronix

TDS8200. The oscilloscope processes the data and display the impulse response of the target.

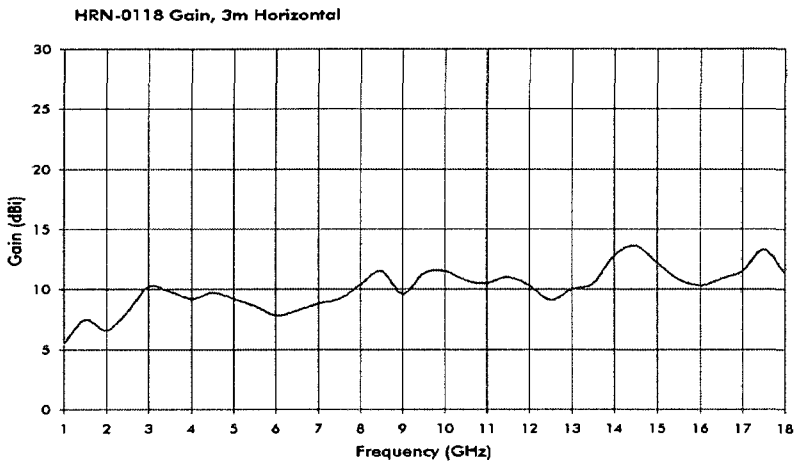

Fig2.3 The gain of the double ridged horn antenna with respect to frequency
(From http://www.tdkrfsolutions.com/WebDataSheets/HRN0118WebSheetGraphs.htm)

Below is the component list of the short-pulse radar system:

- Picosecond Pulse Generator, model 4015D (repeat rate 500kHz)
- Tektronix TDS8200 Digital Sampling Oscilloscope
- Three HRN-0118 double ridged horn antennas
- Microwave switch PE7158
- Microwave signal amplifier AML218L3402
- Programmable Power Supply GW PPT-3615
- National Instruments GPIB-USB-HS
- Cables
- 3/4"plywood to imitate the wall

The whole impulse radar system flow chart and hardware configuration are shown in Fig 2.4.

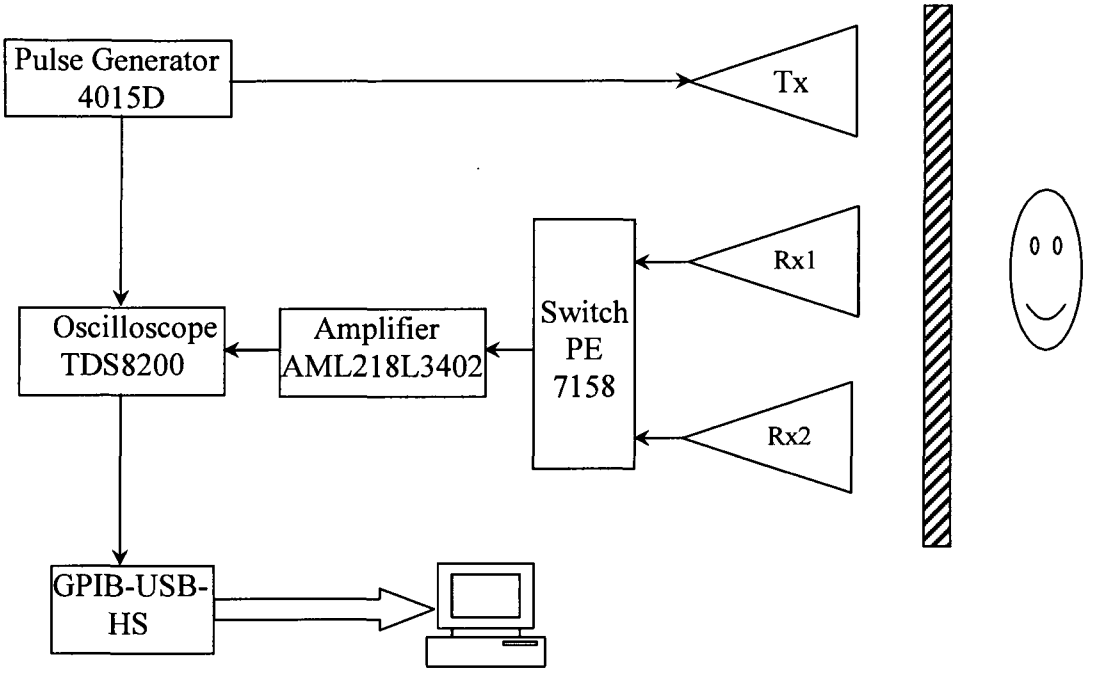

Fig2.4 The flow chart of the Short-Pulse radar system

2.3 Data acquisition

In order to process the data of the impulse response, we need to collect the real-time data from TDS8200. In this part we develop the data acquisition software by Labview. Labview is a graphical programming software which is very powerful in automated test, instrument control and data acquisition.

The GPIB interface NI IGPIB-USB-HS is used to connect the digital sampling oscilloscope TDS8200 and the computer, so we can control the microwave switch PE7158 and the data acquisition automatically. The data from the oscilloscope can be saved directly to the computer for later processing. Fig2.5 shows the interface of the automatic control software.

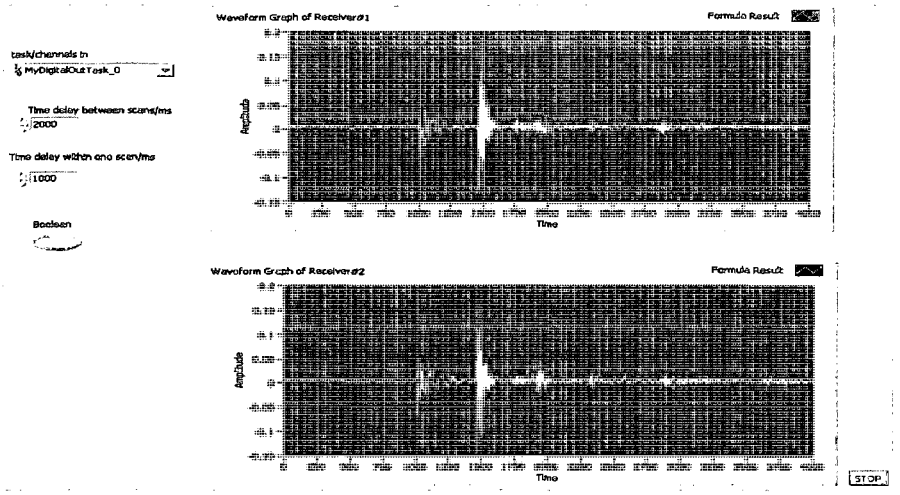

Fig2.5 Data acquisition software interface developed by Labview

2.4 Range measurement

A 2.4m×1.2m×3/4" plywood board is set between the radar and the target at a distance of 1m from the antenna to simulate a wall. The target is a metallic reflector and set on the chair behind the board at d=1.3, 1.6, 1.9m from the antenna (suppose the target only moves alone the normal direction). Fiure2.6 shows the location of antenna, board and target.

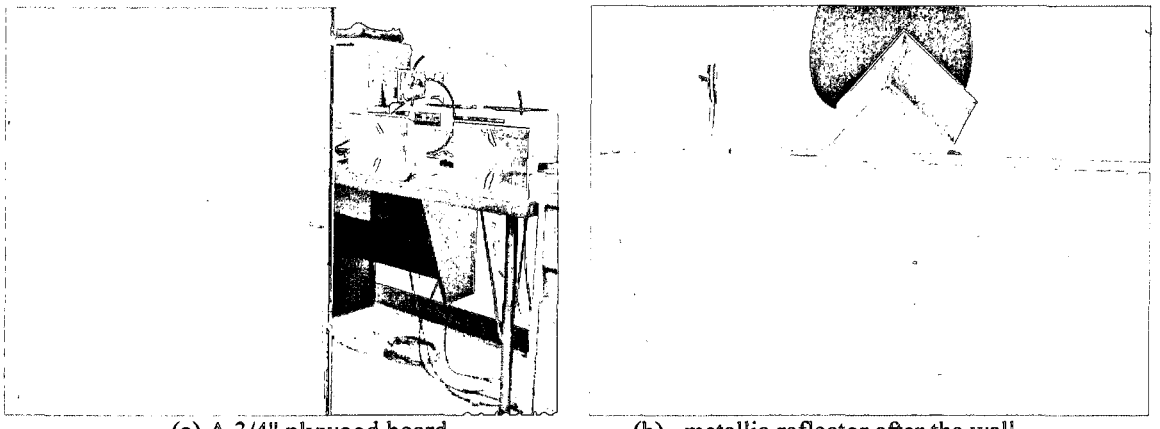

(a) A 3/4" plywood board (b) metallic reflector after the wall

Fig2.6 The target and the 'wall'

Fig2.7 shows the impulse response when the target was put behind the plywood board at d=1.3, we can see the response from the coupled signal between transmitter and

receiver, the response from the plywood wall and finally the backscattering signal from the target. This follows the sequence that the microwave hit those three parts.

In order to make the signal from the target more distinct, the background subtraction is introduced. Fig 2.8 shows the background signal, which mainly includes the coupled signal, signal from the plywood wall. Fig2.9 shows the target after the background subtraction at d=1.3m.

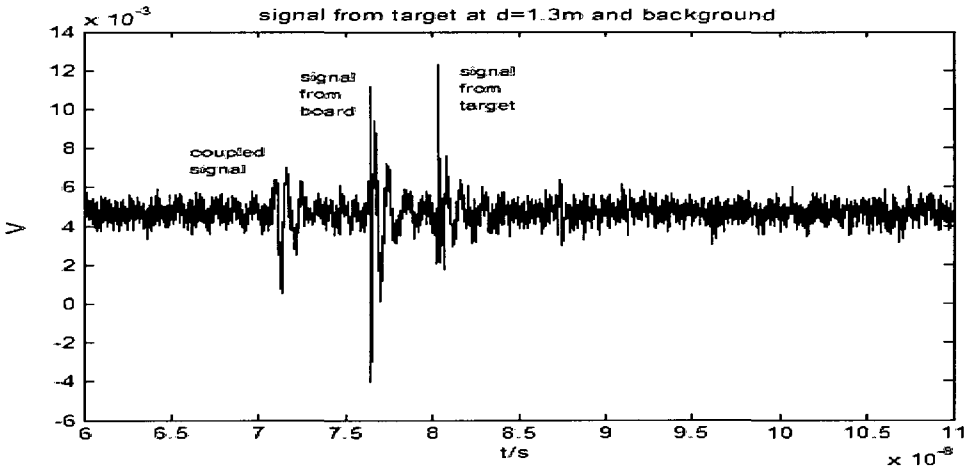

Fig2.7 The response of the target at d=1.3m together with background

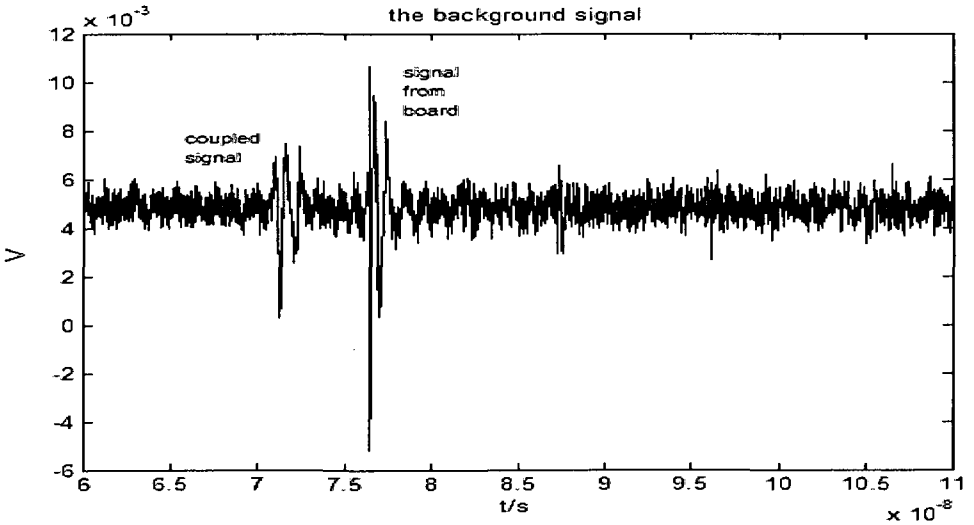

Fig2.8 The response of the plywood board (as background)

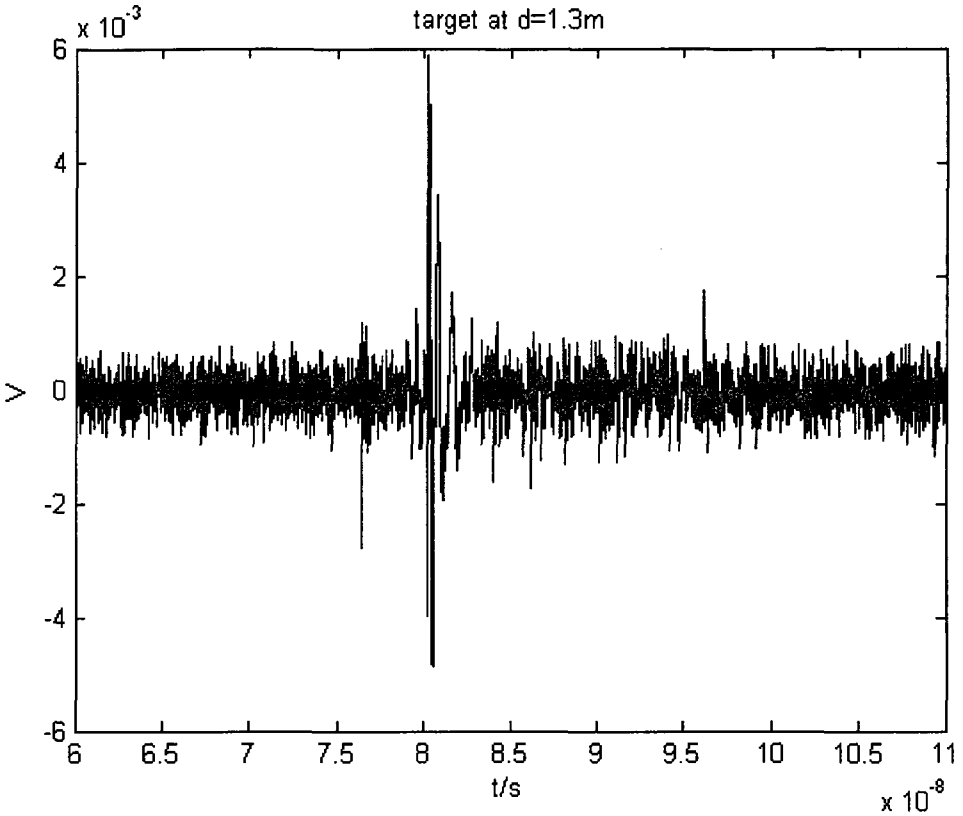

Fig2.9 The response of the target at d=1.3m after subtraction the background

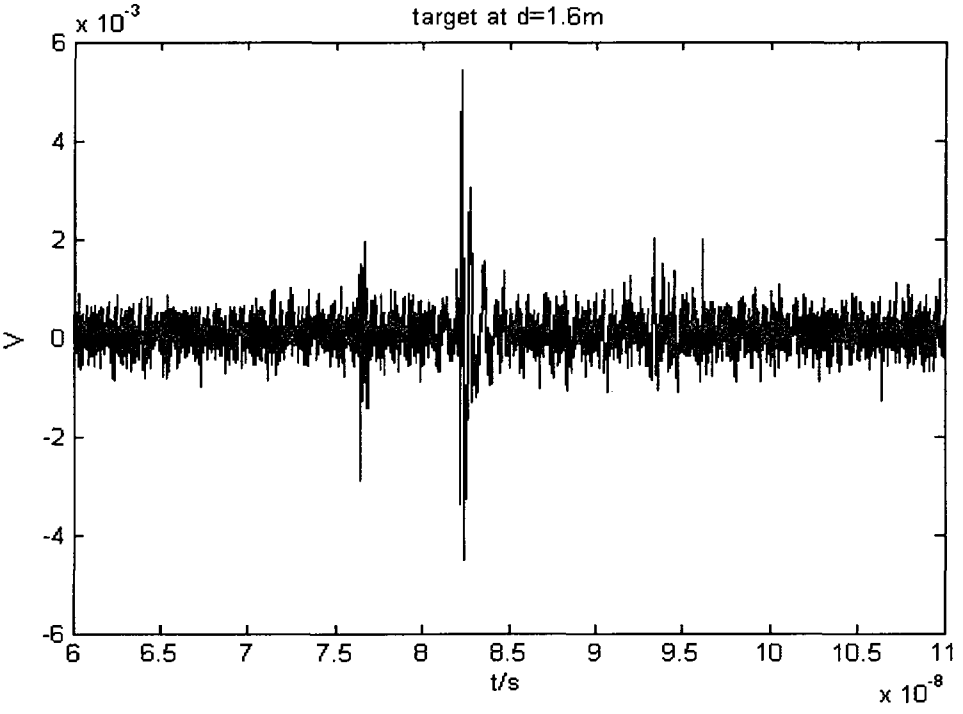

Fig2.10 The reflector is at a distance of 1.6m from the antenna (after -background)

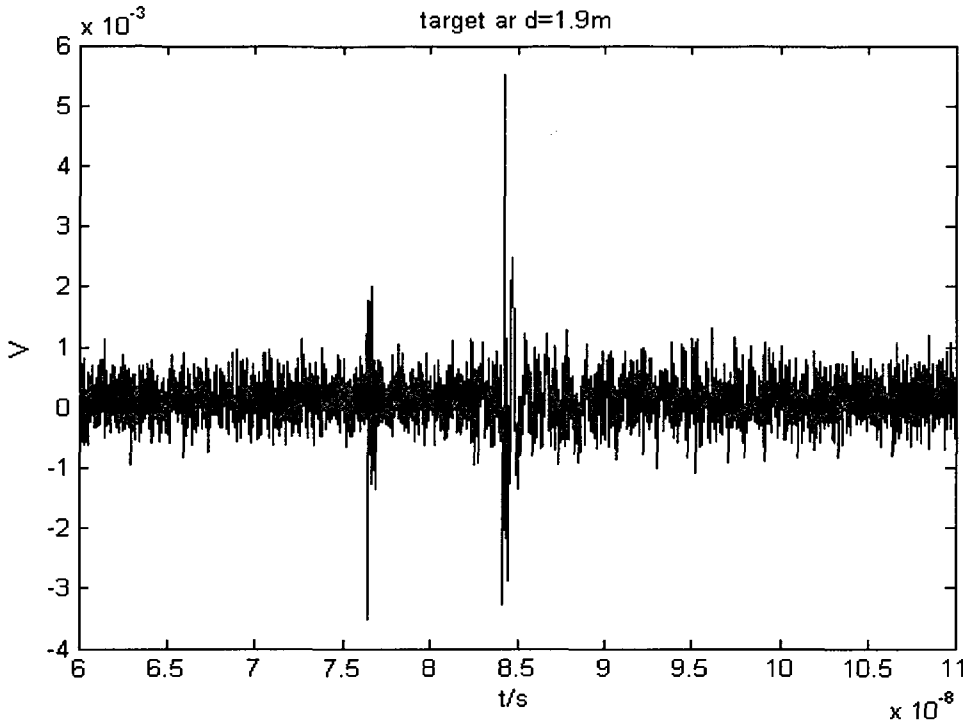

Fig2.11 The reflector is at a distance of 1.9m from the antenna (after -background)

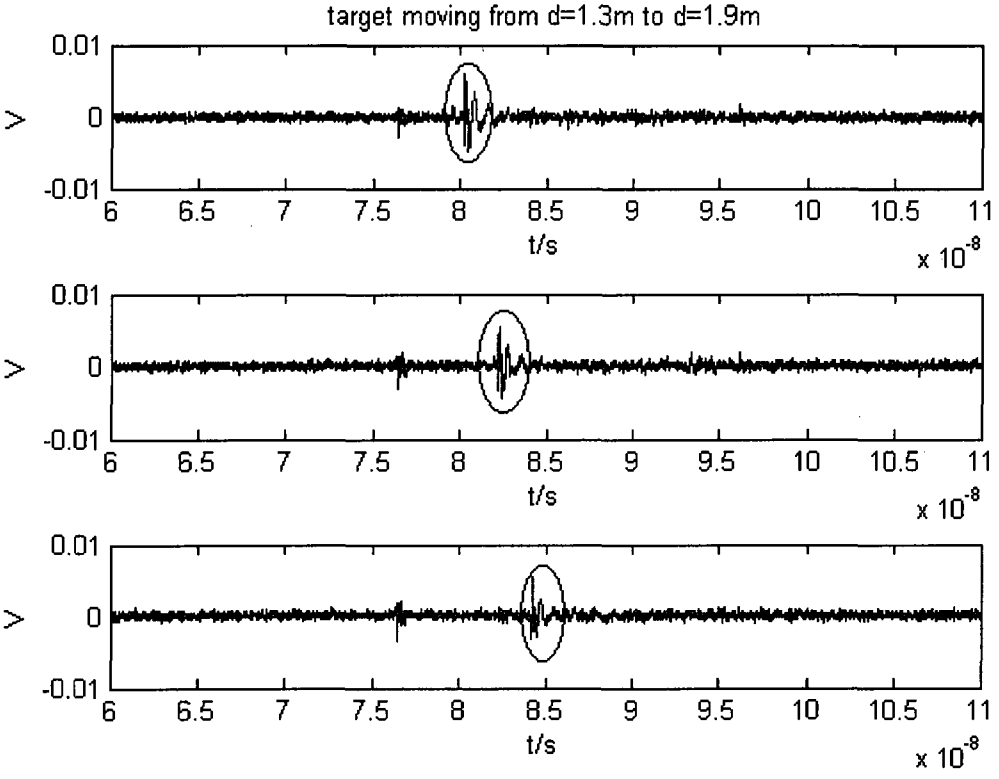

Fig 2.12 Measured range profile for a target at three distances: d=1.3m, 1.6m, 1.9m

Fig2.9 to Fig2.12 show the response of the reflector at d1=1.3m, d2=1.6m, d3=1.9m respectively. The response of the targets come up at t1=80.2ns, t2=82.2ns, t3=84.2ns. If we take d1=1.3m as the reference position, then

$$d2' = d1 + \frac{c}{2}(t2 - t1) = 1.3\text{m} + 0.3\text{m} = 1.6\text{m}$$

$$d3' = d1 + \frac{c}{2}(t3 - t1) = 1.3\text{m} + 0.6\text{m} = 1.9\text{m}$$

So, $d2', d3'$ are exactly the same as d2 and d3, we can see that the short pulse radar has a high resolution to detect the range of the target.

2.5 Elliptic curve intersection method

In this part, we will use two receivers to get the azimuth of the target. Since it is easy for us to get the distance of the target using short-pulse radar, we can get the exact location of the target if we know the azimuth.

2.5.1 Analytic math derivation

The ellipse curve intersection (ECI) method [10] is a straight forward method to determine the location of the target by searching the intersection of the two ellipses if we employ two receivers, as shown in Fig2.13.

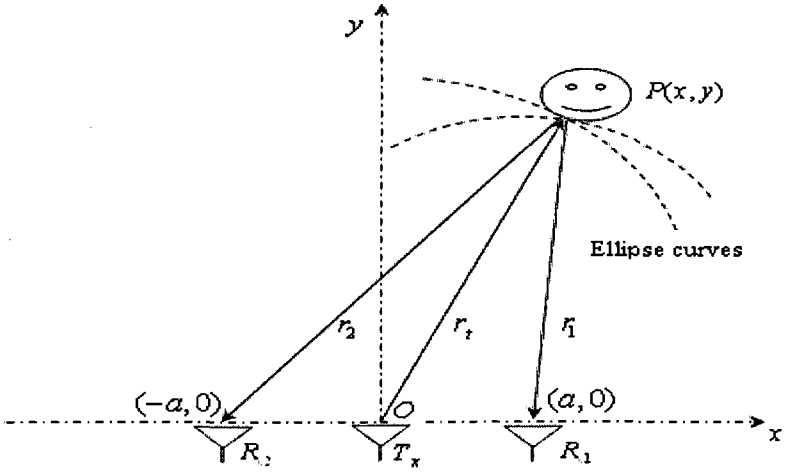

Fig2.13 Elliptic curve method

So the equation of the ellipse with focuses Tx and Rx1, and the equation of the ellipse with focuses Tx and Rx2 are given as follows:

$$\begin{cases} \dfrac{(x-a/2)^2}{(c\tau_1/2)^2}+\dfrac{y^2}{(c\tau_1/2)^2-(a/2)^2}=1 \\ \dfrac{(x+a/2)^2}{(c\tau_2/2)^2}+\dfrac{y^2}{(c\tau_2/2)^2-(a/2)^2}=1 \end{cases} \tag{2.1}$$

By solving the two simultaneous equations above, we can get the location of the target.

The simultaneous equations (2.1) give the solution of the target location (x, y), however this is only true on the condition that the wall effects could be ignored, which means that the wall has small thickness or low permittivity. In practice, usually the wall can not be ignored due to its insertion loss, phase distortion and refraction. The ray tracing of the impulse through-wall radar in the real application is given in Fig2.14. In Ma Lin and Zhang zhongzhao' paper [10], the virtual elliptic curve imaging (VECI) method was proposed.

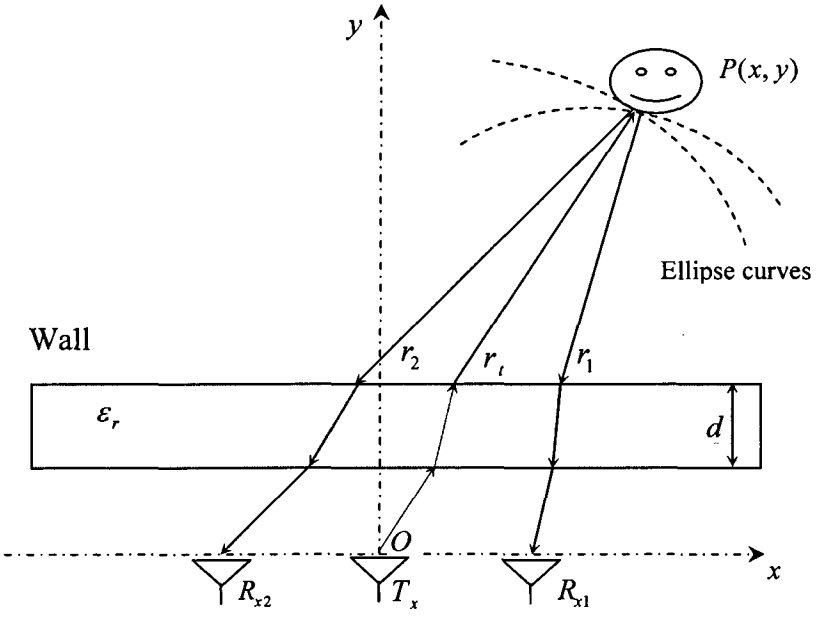

Fig2.14 The ray tracing of impulse through -wall radar

In order to get the accurate location of the target by impulse through wall radar, it is necessary to do more research on the microwave propagation through the wall, especially to calculate the full routine of the wave propagation in side the wall. Fig2.15 shows the geometry of wave propagation through the wall.

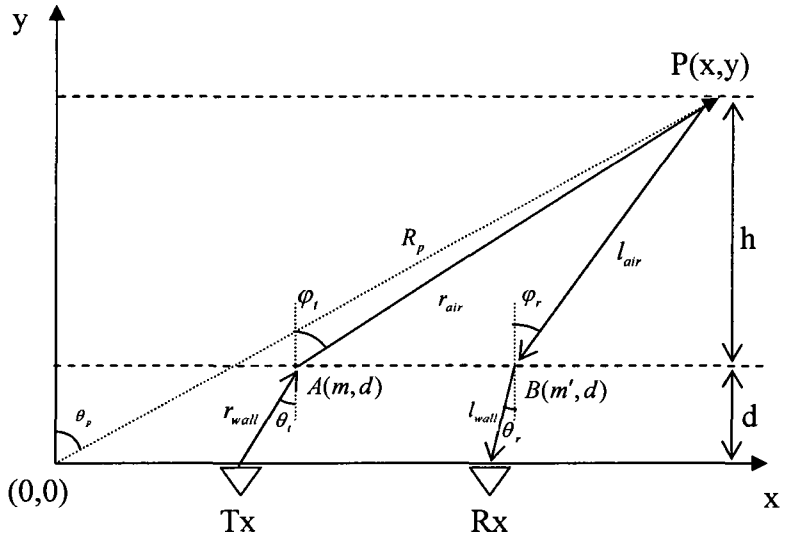

Fig2.15 The geometry of wave propagation through the wall

Point A and B are the virtual focuses of the elliptic curve. Suppose d is the thickness of the wall and ε_r is the wall dielectric constant. As discussed in chapter one, the microwave propagation velocity in the wall $v = c/\sqrt{\varepsilon_r}$, so the totally time of arrive τ_p is given by:

$$\tau_p = \tau_{p,air} + \tau_{p,wall}$$

$$= \frac{r_{air} + l_{air}}{c} + \frac{r_{wall} + l_{wall}}{v}$$

$$= (h/c\cos(\varphi_t) + h/c\cos(\varphi_r)) + (\sqrt{\varepsilon}d/c\cos(\theta_t) + \sqrt{\varepsilon}d/c\cos(\theta_r)) \qquad (2.2)$$

The forward microwave propagation path follows

$$\begin{cases} x = m + h\tan\varphi_t \\ \sin\varphi_t = \sqrt{\varepsilon_r}\sin\theta_t \\ \tan\theta_t = (m - Tx)/d \end{cases} \tag{2.3}$$

While the inverse path of the microwave propagation follow equation (4),

$$\begin{cases} x = m' + h\tan\varphi_r \\ \sin\varphi_r = \sqrt{\varepsilon_r}\sin\theta_r \\ \tan\theta_r = (m' - Rx)/d \end{cases} \tag{2.4}$$

There are eight variables in equation (2), (3) and (4): $x, h, \theta_t, \varphi_t, \theta_r, \varphi_r, m, m'$, with seven independent equations in equation (2), (3) and (4), it seems we can not solve these equations, however, by employing another receiver, we have another seven independent equations but six unknowns this time (because x, h are the same).

In conclusion, by employing two receivers, there are fourteen unknowns and fourteen independent equations. Consequently, the target coordinates(x, h) can be solved.

2.5.2 Target locating

Table2.1 Comparison of measured data and real data

Receiver1		Receiver2		X /cm	/m	Y/m /cm	/m	R /cm	/m	θ/rad	
t/ns	r/m	t/ns	r/m	Meas value	Real value	Meas value	Real value	Meas value	Real value	Meas value	Real value
82.6	24.7628	81.8	24.5230	-53.1624	-0.6	148.918	1.5	158.1228	1.6155	1.9137	1.9513
81.8	24.5230	81.6	24.4630	-12.7113	-0.2	149.777	1.5	150.3155	1.5133	1.6555	1.7033
81.6	24.4630	81.9	24.5530	19.1559	0.2	149.875	1.5	151.0945	1.5133	1.4437	1.4382
81.9	24.5530	82.7	24.7928	53.6495	0.6	150.355	1.5	159.6400	1.6155	1.2281	1.1903
82.8	24.8228	84.4	25.3024	119.5788	1.0	134.431	1.5	179.9189	1.8028	0.8428	0.9828

Table2.1 gives us some measurement data regarding one moving target. In this experiment, we measured the moving targeting at five different locations. The time delay at each location is recorded by both receiver 1 and receiver 2. Applying ECI method, we

can get the exact location of the target at each position. Some measurement values and real values are also listed in Table 2.1.

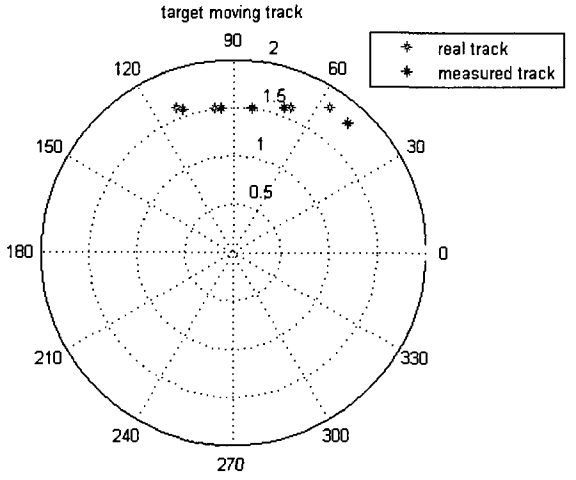

Fig 2.16 The target moving track detected by short-pulse radar

Fig2.16 shows the polar chart of the target locations. The original of the polar chart is the impulse radar system and the beam direction of the impulse radar is at 90 degree. The red asterisks show the real locations of the target, while the blue asterisks indicate the measured locations of the target. From the figure above we can see that the measured location and the real location match well around the beam direction of the impulse radar, however, they mismatch a little bit when the target locations are off the main radar beam.

2.5.3 Impulse radar imaging by 1-D scanning

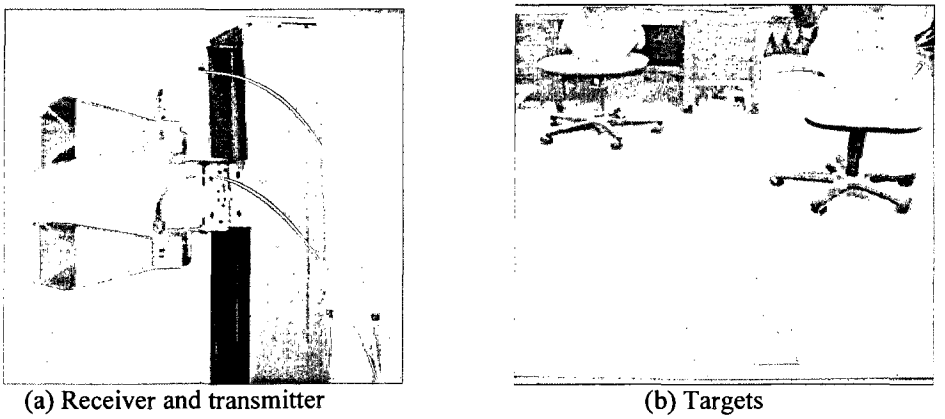

(a) Receiver and transmitter (b) Targets

Fig2.17 The target moving track detected by short-pulse radar

Fig.2.17 shows the antenna and target locations: The transmitter and receiver are mounted in the inverse 'T' planar scanner, and the targets comprise two metallic reflectors. The step motor of the scanner are controlled by Labview to achieve horizontal dimension scan from 0.11m to 1.51m, totally 128 equi-paced points, meanwhile, the data measured by TDS8200 is automatically collected by GPIB connection with PC. The locations of the targets are given in Table 2.2.

Table2.2 The location of the targets

	x/m	y/m	z/m
The left one	0.44	2.43	0.73
the right one	1.18	1.74	0.74

Fig2.18 shows the range profile of the target as a function of scan position. The horizontal axis is the number of the scan, while the vertical axis is the range. Figure 2.18(a) and (b) show the ideal curve and experimental curve respectively. Fig2.19 shows the final image constructed by ECI methods.

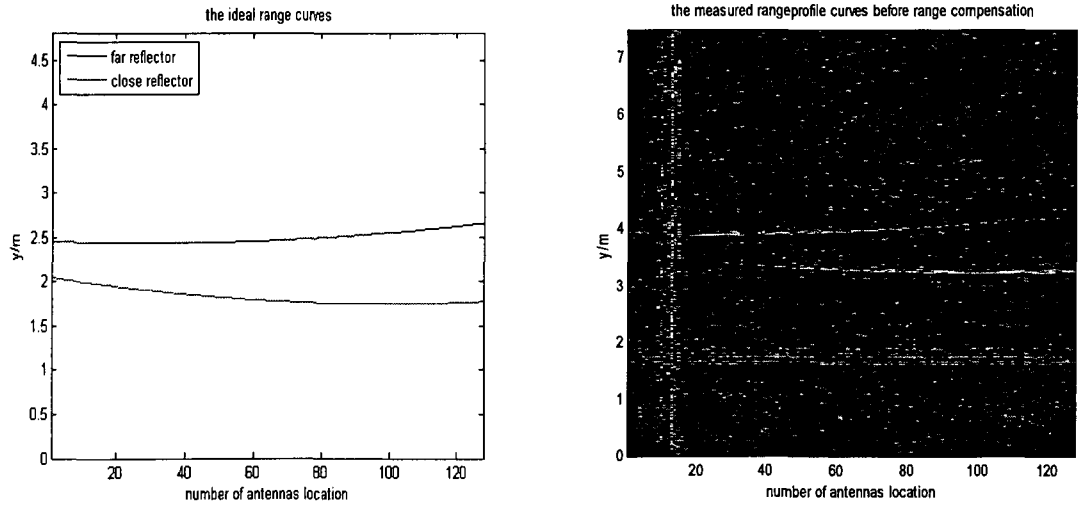

(a) The ideal range curve (b) The experimental curve

Fig2.18 The range profile as a function of scan position

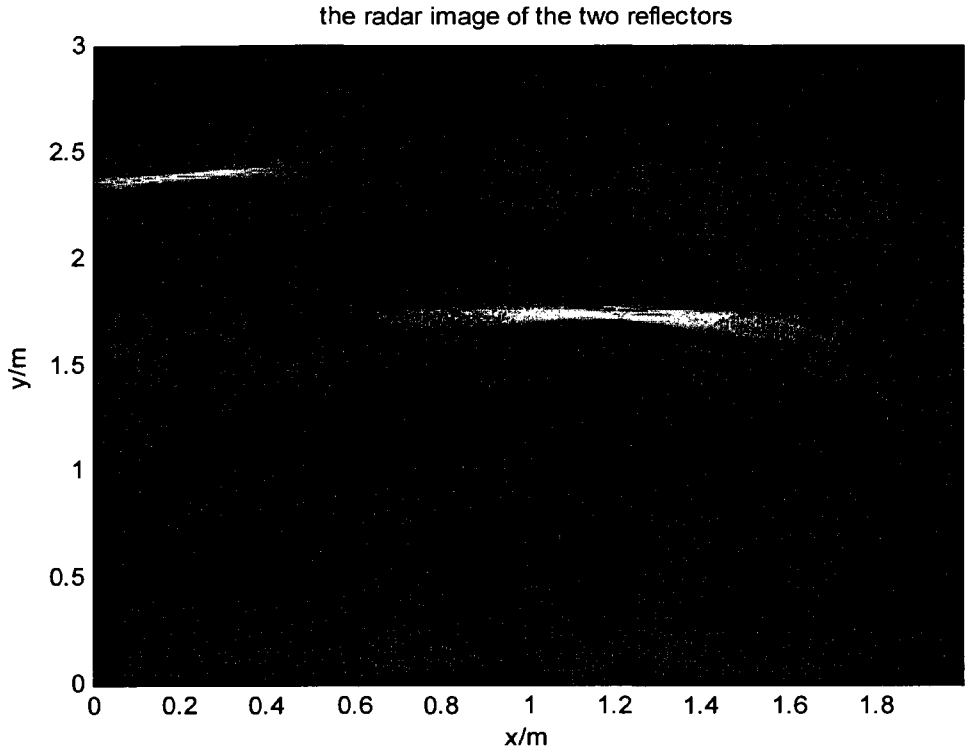

Fig2.19 The image result of the target by employing ECI method

2.5.4 Experiment of target tracking

In this experiment, a person holding a metallic reflector walked behind the plywood wall in a routine like "⋈". Fig2.20 shows one image frame of the elliptic curve intersection results. There are two curve intersections in Fig2.20, the upper and strong one shows the location of the plywood board, while the lower and weaker one shows the location of the target.

Fig2.21 shows the ground truth track of the target and the track extracted from the image sequences. Detected locations agree well to the ground truth pattern. A video clip has also been created to capture the whole trajectory of the moving target.

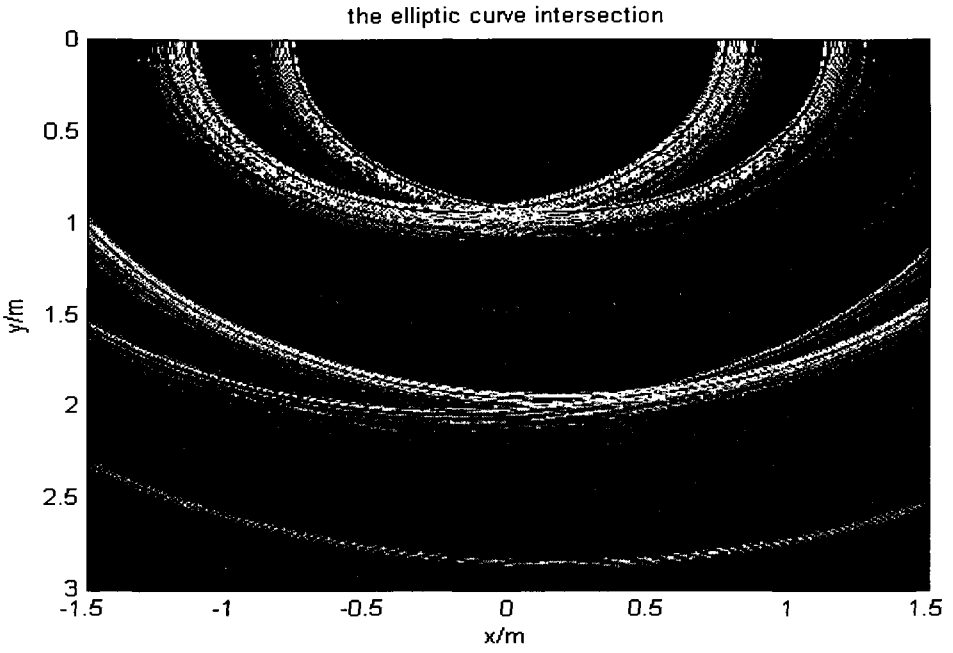

Fig2.20 The location of one person

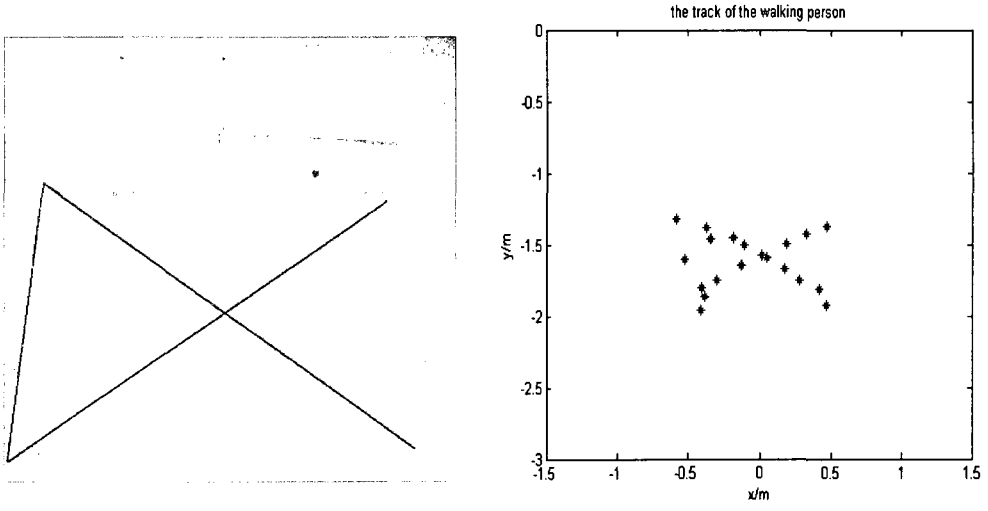

(a) The really walking path (b) the measured result

Fig2.21 The track of the walking person

CHAPTER 3

SWEPT FREQUENCY THROUGH-WALL RADAR SYSTEM

3.1 Introduction

In this chapter, we study the performance of a swept frequency through-wall radar system. First we give the hardware configuration of the swept frequency radar, second the range profile is derived theoretically from the data in frequency domain. In the following, we form the imaging of the targets by two methods. Last, the dynamic target detection is presented.

3.2 Hardware configuration

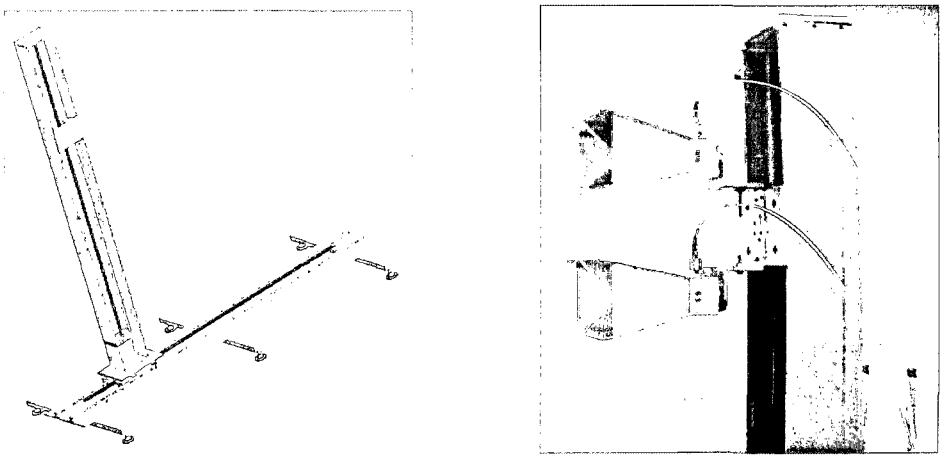

(a) The general view of the inverse 'T' scanner (b) The mounted transmitter and receiver

Fig3.1 The schematic of the 2-D scanner

The hardware configuration is shown in Fig3.1. Fig3.1 (a) shows the prototype of the inverse 'T' scanner, which is used to mount the transceiver. This scanner is driven by

two step motors in both horizontal direction and vertical direction, so the transmitter and receiver can move in the x-y plane.

3.3 Data acquisition

The Agilent 8719ET network analyzer is connected to the computer by GPIB-USB-HS, so the S21 data measured by Agilent 8719ET network analyzer can be collected and saved automatically by Labview software.

3.4 Range profile

3.4.1 Range profile in frequency domain

In chapter 2, the range profile of the targets under measurement can be easily obtained by the digital oscilloscope TDS 8200.It is very straight forward in the time domain, however, it can also be derived using the backscattering data in the frequency domain. Suppose our target is distributed in the range dimension as showed in Fig3.2.

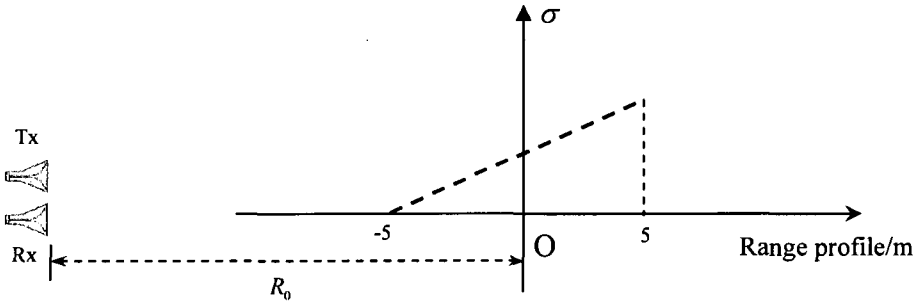

Fig3.2 The model of measuring range profile in the frequency domain

Suppose the start frequency of the radar system $f_1 = 1GHz$, the stop frequency $f_2 = 5GHz$. The target can be modeled as ideal scatters, which distributes in the range domain from -5 meter to +5 meter with a linear scattering intensity distribution from 0 to 100 as shown in Fig3.3.

Assuming the incident electrical field $E_i = \exp(j2\pi ft)$, then the backscattering signal is

$$E_s(f) = \sum_i \sigma_i \exp(j2\pi f(t - \frac{2(R_0 + x_i)}{c})) \qquad f \in (f_1, f_2) \tag{3.1}$$

By removing the time factor $\exp(j2\pi ft)$, equation (3.1) can be simplified as follows:

$$E_s(f) = \sum_i \sigma_i \exp(-j\frac{4\pi f}{c}(R_0 + x_i)) \qquad f \in (f_1, f_2) \tag{3.2}$$

Then the factor $\exp(-j\frac{4\pi f}{c}R_0)$ in equation (3.2) can be compensated by multiplying the conjugate of itself, for it has no relation with the target distribution, so

$$\begin{aligned} E_{sc}(f) &= E_s(f) * \exp(j\frac{4\pi f}{c}R_0) \\ &= \sum_i \sigma_i \exp(-j\frac{4\pi f}{c}x_i) \\ &= \sum_i \sigma_i \exp(-jkx_i) \quad k \in (k_1, k_2) \end{aligned} \tag{3.3}$$

Here $k = 4\pi f / c$, is the wave number. $(k_1 = 4\pi f_1 / c \quad k_2 = 4\pi f_2 / c)$

3.4.2 Fourier Transform

The 1-D Fourier Transform pair is showed as equation (4.4):

$$\begin{cases} H(jf) = \int h(t) * \exp(-j2\pi ft)dt \\ h(t) = \int H(jf) * \exp(j2\pi ft)df \end{cases} \tag{3.4}$$

By employing the inverse Fourier Transform on equation (3.3), the range profile can be derived, the detailed derivation is showed below:

$$r(x) = \int_{k_1}^{k_2} \sum_i \sigma_i \exp(-jkx_i) * \exp(jkx) dk$$

$$= \int_{k_1}^{k_2} \sum_i \sigma_i \exp(jk(x - x_i)) dk$$

$$= \sum_i \sigma_i \frac{\exp(jk(x - x_i))}{j(x - x_i)} \Bigg|_{k_1}^{k_2}$$

$$= \sum_i \sigma_i * (k_2 - k_1) * \sin c[\frac{k_2 - k_1}{2}(x - x_i)] * e^{j\frac{k_2 + k_1}{2}(x - x_i)} \quad (3.5)$$

When the bandwidth becomes infinitely large, which means$(k_2 - k_1) \Rightarrow \infty$, equation (3.5) simplifies as

$$r(x) = \sum_i \sigma_i * \delta(x - x_i) \quad (3.6)$$

Equation (3.6) shows the ideal range profile on the condition that the bandwidth is infinite large. However, the bandwidth is limited in practical, so the delta function in equation (3.6) will degrade to sinc function in equation (3.5), which blurs the image due to the side lobe of itself.

3.4.3 Matlab simulation

Parameter settings

Frequency: 1-5GHz

Frequency Sample Number: $N_f = 401$

Target Location: $x \in (-5,5)m$

Number of Scatters: $N_s = 51$

Scattering Intensity: $\sigma \in (0,100)$

Fig3.3 shows the backscattering data simulated in the frequency domain. Fig3.4 gives the range profile after imposing the inverse Fourier Transform. The oscillations between the spikes are caused by the sidelobe of sinc function as shown in equation (3.5).

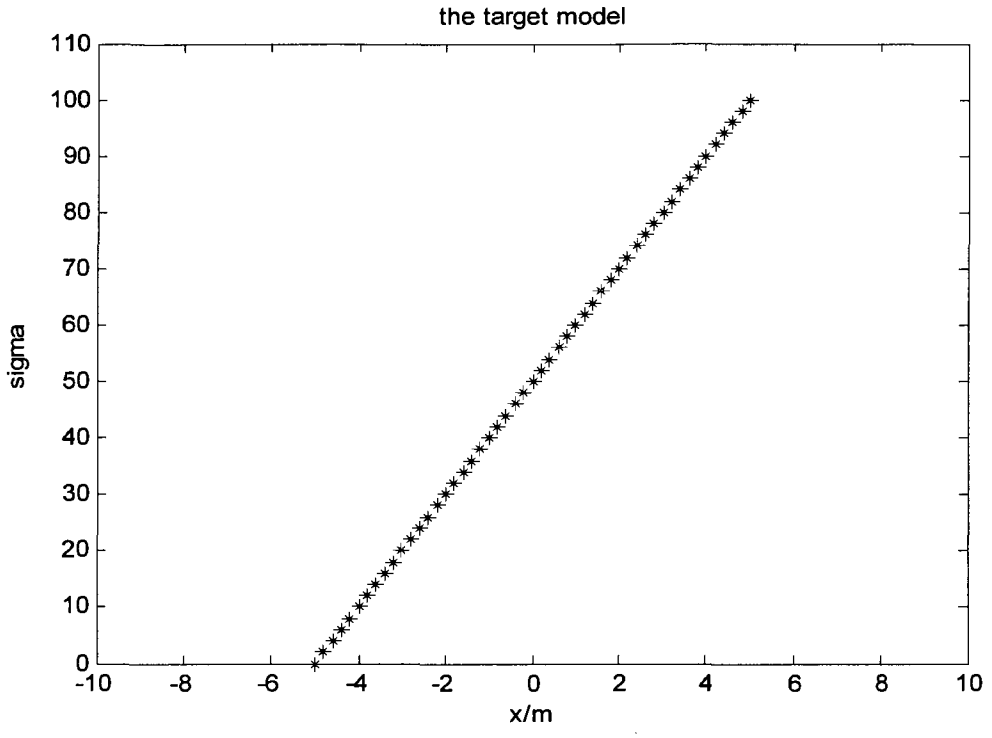

Fig3.3 The target model

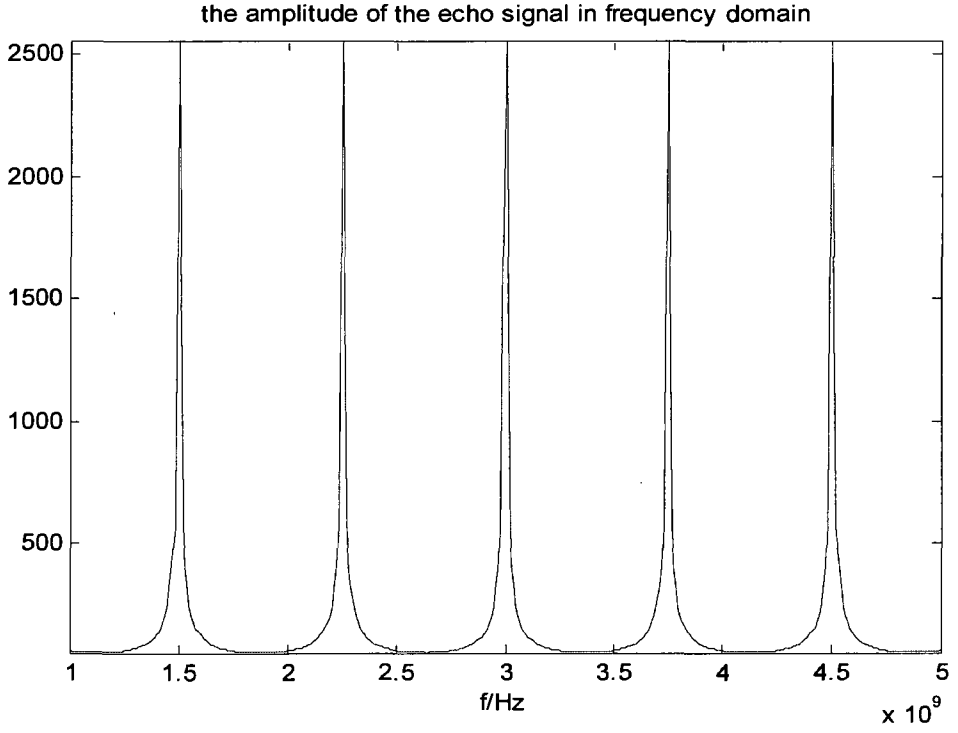

Fig3.4 The amplitude of the backscattering signal

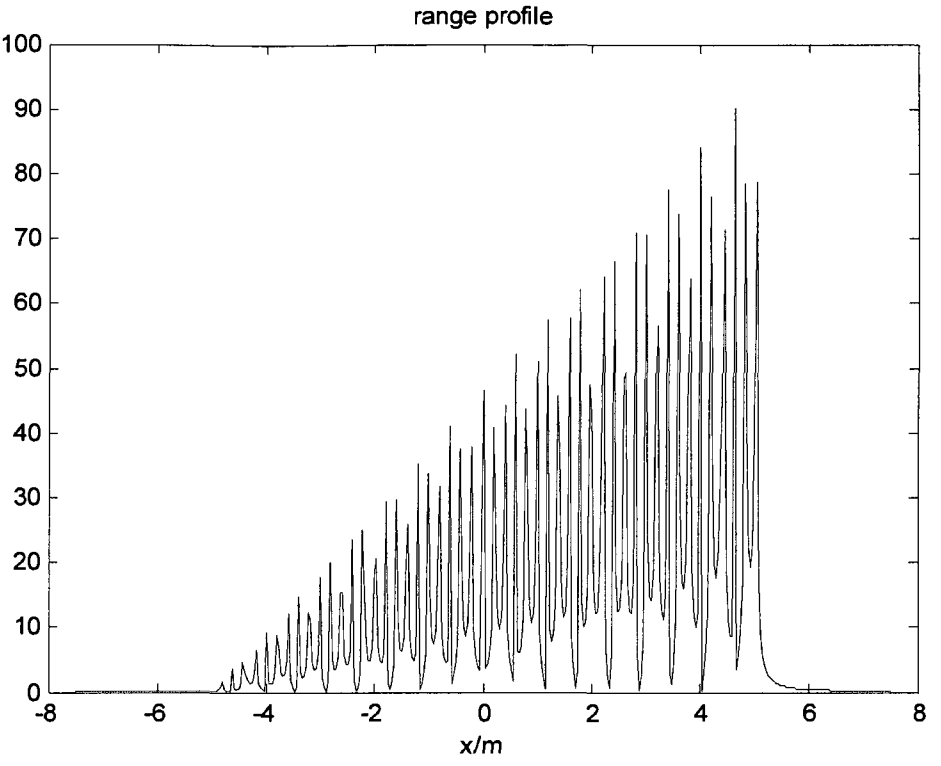

Fig3.5 The reconstructed range profile

3.5 2-D Imaging

In this section, we examine the 2-D imaging capacity of the swept frequency radar system. Two corner reflectors are put in front of our radar system as the targets under test. The targets location is the same as Table2.2. The step motor of the scanner are controlled by Labview to achieve horizontal dimension scan from 0.11m to 1.51m , totally 128 equi-paced points, meanwhile, the data in Agilent8719ET is automatically collected by GPIB connection using PC.

The parameter settings of the network analyzer are listed below:

Measurement:	Transmission (S21)
Power:	5dBm
Frequency	1GHz -13.5GHz

Number of Frequency: Point 401

Data format: Real Part and Imagine Part

Range resolution: dr=1.2cm

3.5.1 2-D image by Elliptic Curve Imaging Method

To get the 2-D image by curve intersection method, first we have to get the range profile of the target at each scanning position. Simply this step can by easily accomplished by the inverse Fourier transform as we discussed in 3.4.2. Fig3.7 shows a range profile of the target at an arbitrary location.

Since the target location and the antennas locations are known, mathematically, we can calculate the ideal range curves of the two corner reflectors as a function of each scanning point. Fig3.8 shows the ideal curves of each reflector. Fig3.9 shows the measured range profile which indicates a great match to Fig3.8.

Finally, the 2-D image can be got by curve intersection method as shown in Fig3.10.

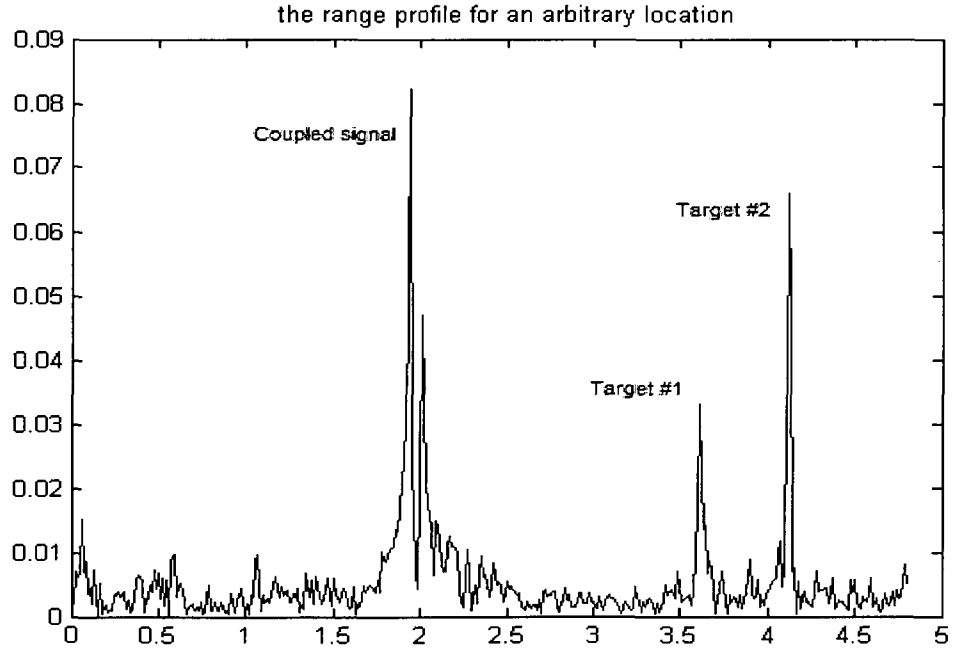

Fig3.6 The range profile of the target at an arbitrary location

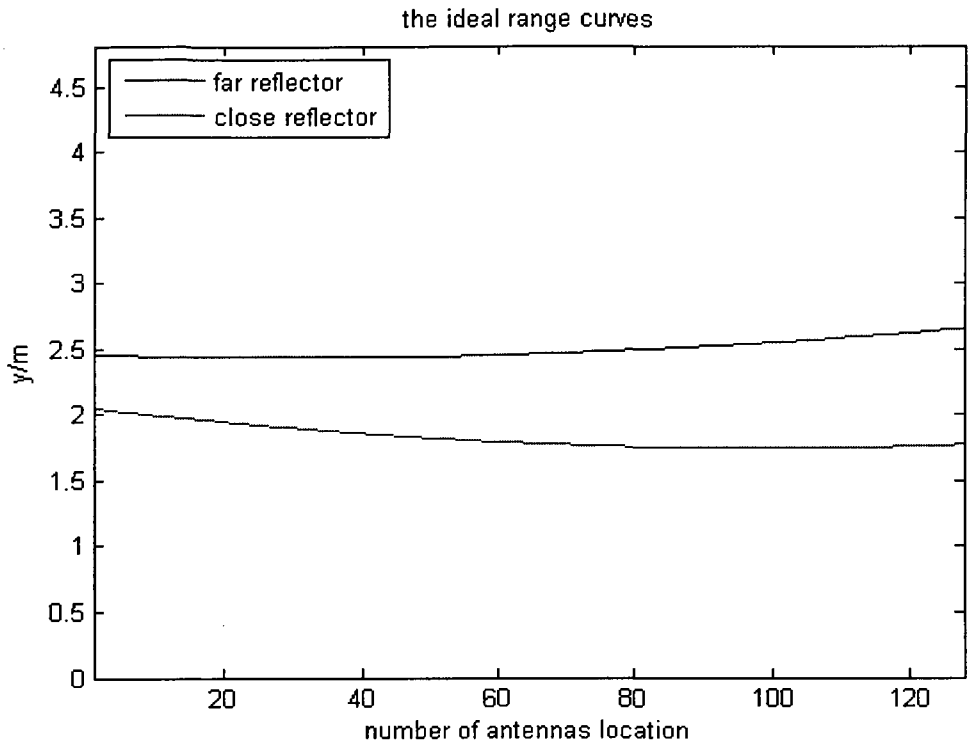

Fig3.7 The ideal range profile of the two corner reflectors

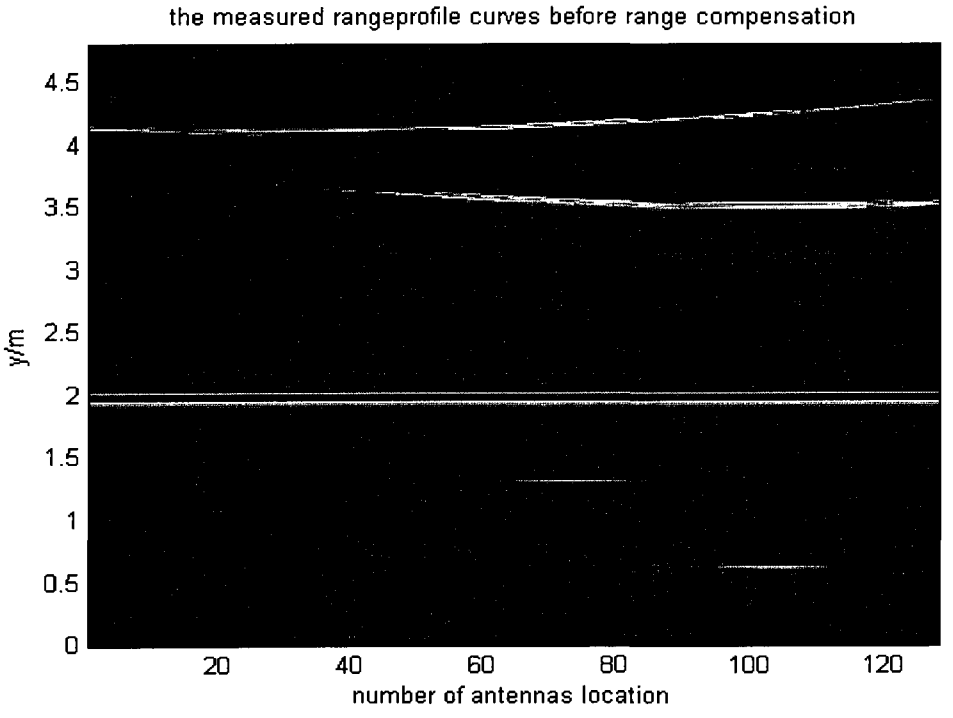

Fig3.8 The measured range profiles of the two corner reflectors

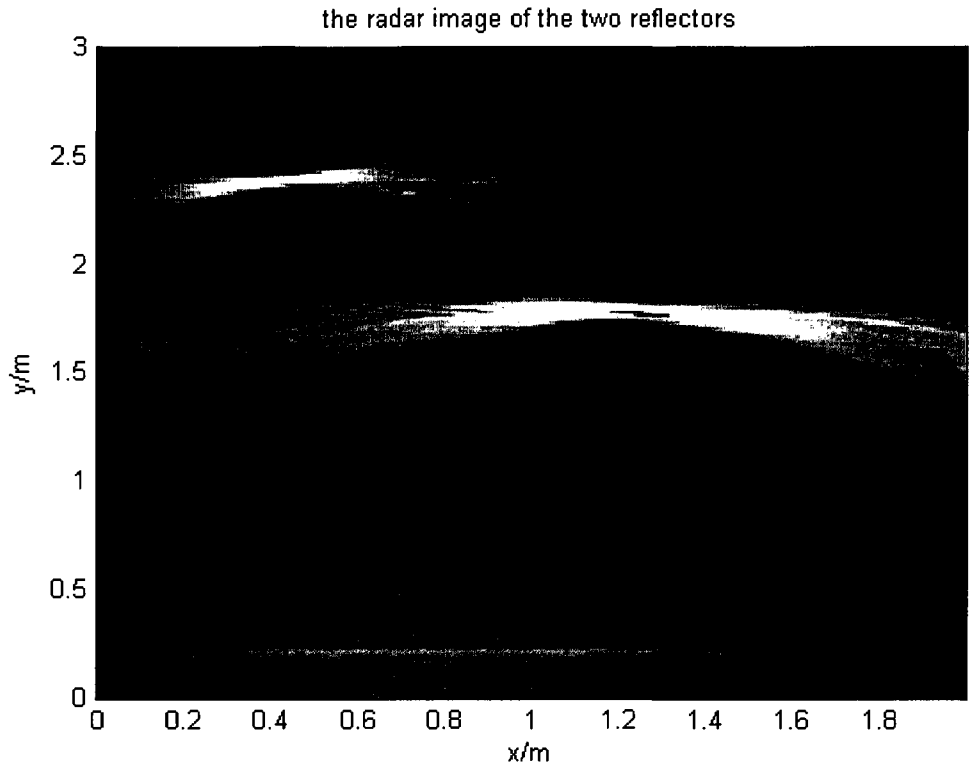

Fig3.9 The 2-D image of the two corner reflectors by curve intersection method

3.5.2 2-D image by Adaptive Feature Extraction

In the curve intersection method to form the 2-D image, only the amplitude of the range profile is considered. We lose the phase information in the data collected from the vertical network analyzer, in order to explore the full potential of the backscattering data, the adaptive feature extraction algorithm is employed to form the 2-D image of the two metallic reflectors.

The method assumes that any electromagnetic target can be represented by multiple ideal scatters. We try to locate each scatter that constitutes the targets. The basic procedures of the adaptive feature extraction are [9]:

1. Initialize residue signal Er=Es, Es is the total scattering field
2. Locate the position of a unit point scatterer by maximizing the projection of point

scatter response and the residue signals onto the

$(x,y) = \arg\max < \exp(-j2\pi f \cdot d(x,y)/c), E_s >$, where $d(x,y)$ is the round trip distance from the radar to the scatterer

3. The strength of the scatterer is found by

$$\sigma(x,y) = \frac{< \exp(-j2\pi f \cdot d(x,y)/c, E_s >}{< \exp(-j2\pi f \cdot d(x,y)/c, conj(\exp(-j2\pi f \cdot d(x,y)/c) >}$$

4. The strength of the scatterer is found and its response extracted from the radar data , $E_r \Leftarrow E_r - \sigma(x,y) * \exp(-j2\pi f \cdot d(x,y)/c)$

5. Repeat steps 2-4 until a preset number of scaterers have been extracted or E_r energy is below some threshold.

Matlab Simulation

In this section, three separate scatters are simulated based on the AFE algorithm. Assuming threes scatters located at (0, 0) m, (0, 0.3) m, (0.3, 0) m with scattering intensity σ =150, 100, 50 respectively. The original target setting is shown in Fig3.10.

After the adaptive feature extraction algorithm, the final image is shown in Fig3.11.

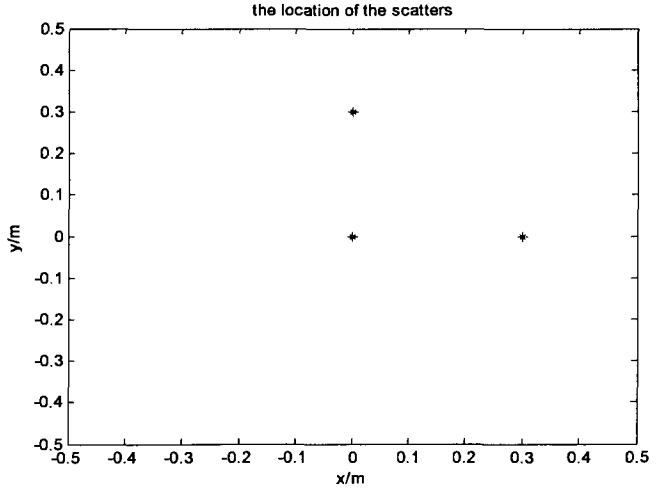

Fig3.10 The location of the three original scatters

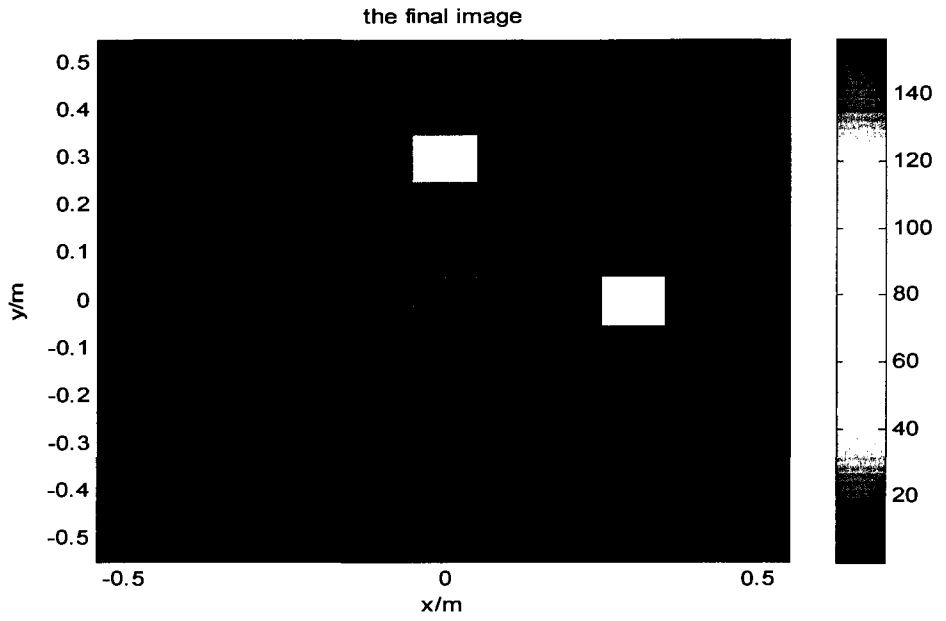

Fig3.11 The final image of the target

Measurement result

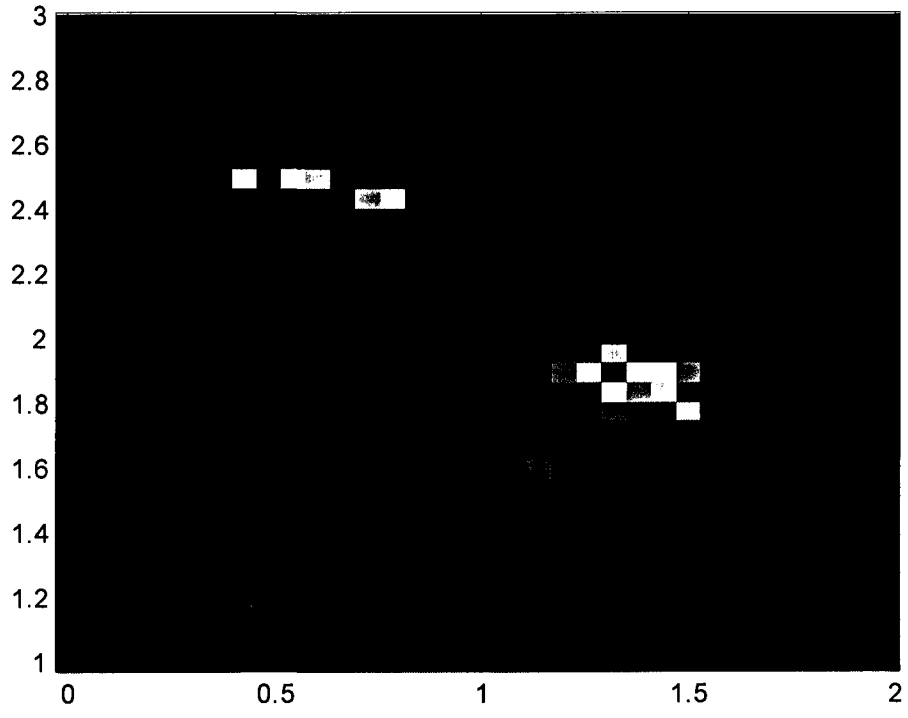

Fig3.12The final image of the two metallic corner reflectors

3.6 Detection of dynamic targets

We also collected data from stationary and moving targets using a swept frequency radar system based on an Agilent vector network analyzer 8719ET (50 MHz-13.5 GHz). The radar is frequency domain UWB (ultra wideband) radar while impulse radar in Section 2.1 is time-domain UWB radar. The list of hardware components is shown below. Fig3.14 shows the block diagram of the VNA-based swept frequency radar at UTPA.

- Agilent 8719ET Transmission/Reflection Network Analyzer (50 MHz-13.5 GHz)
- Range resolution: 1.2 cm
- TDK RF Solutions HRN-0118 double ridged horn antennas
- Microwave power amplifier and low noise amplifier

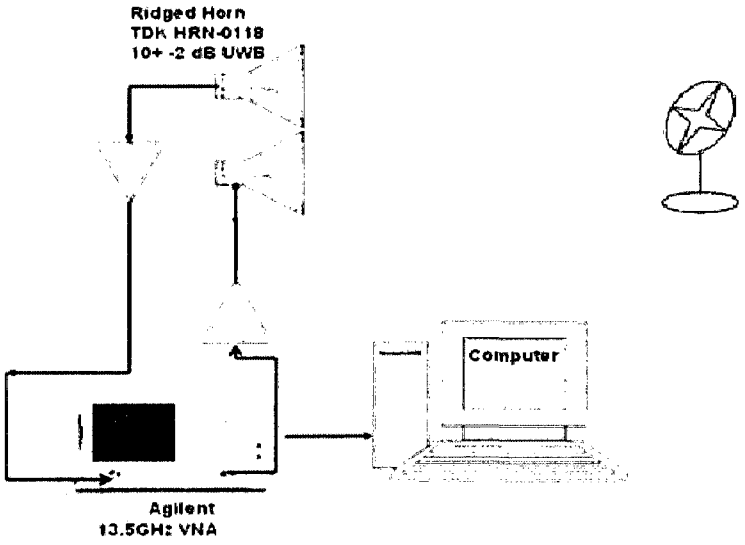

Fig3.13 Block diagram of a VNA-based swept frequency radar at UTPA

If a target moves too fast in relative to the frequency sweeping rate, the network analyzer might lose phase coherence. To test if the swept frequency radar can detect a target not moving too fast, we collected the range profiles of an electric fan with rotating blades off in Fig3.15 and on in Fig3.16. First, we see that the big component due to the

frame of the fan remains the same after the fan is turned on, meaning phase coherence is kept. Second, the extra rotating blade features are quite distinct once the fan is turned on.

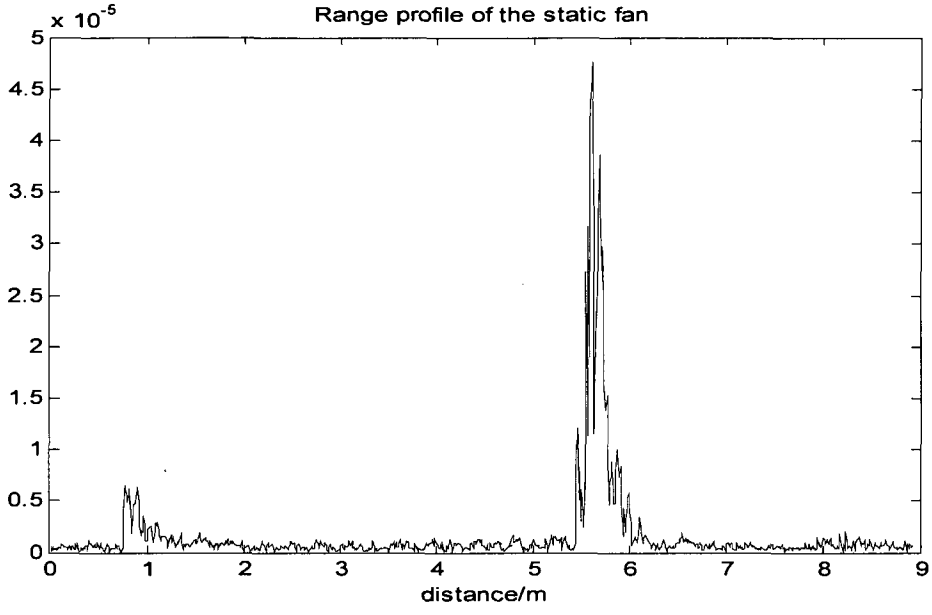

Fig3.14 Range profile of static fan

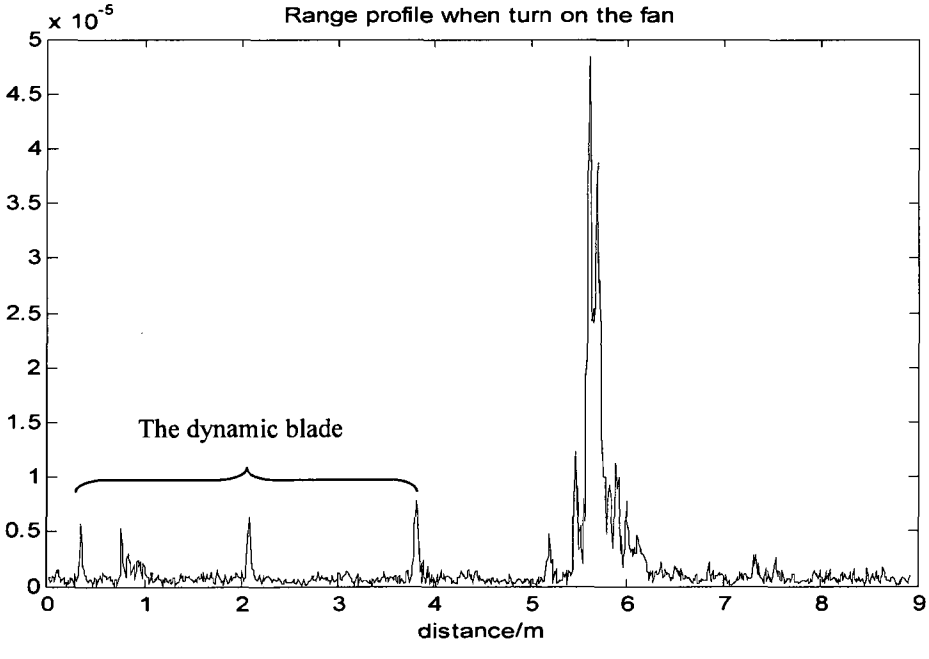

Fig3.15 Range profile of dynamic fan

CHAPTER 4

CONTINUOUS WAVE THROUGH-WALL RADAR SYSTEM

4.1 Introduction

CW radar is very sensitive to detect target motions. It has a high signal-to-noise ratio (SNR) due to its extremely narrow receiver bandwidth. An 882 MHz CW radar system has been used in this chapter. We set out to discriminate different moving targets by their Doppler frequencies and determine their azimuth and elevation angles by direction of arrival (DOA) method [8].

4.2 Definition of Doppler

Doppler is due to the target motion in the boresight of the radar. Suppose the transmitting signal of the radar is $s(t) = A\cos(2\pi f_0 t + \varphi_0)$, and one target is moving in the radar beam at a distance of $d(t)$ from the radar. Then the backscattering signal received by the receiver should be $r(t) = A\alpha\cos(2\pi f_0(t - \frac{2d(t)}{c}) + \varphi_0)$, where α is a decay factor. By taking the derivative of the phase of $r(t)$ with respect to time, we can get the instantaneous frequency:

$$f = \frac{1}{2\pi}\frac{d\varphi}{dt} = f_0 - \frac{2d'(t)}{c/f_0} = f_0 - \frac{2v}{\lambda} \tag{4.1}$$

The Doppler frequency f_d can be defined as the difference between the instantaneous frequency and the carrier frequency, so:

$$f_d = \frac{2v}{\lambda} \quad (v \text{ is the velocity in the beam direction}) \tag{4.2}$$

4.3 CW radar to detect the running fan

In this section, we try to detection the motion of a running fan by CW radar system. Fist, we set up the CW radar system and collect the data by LabVIEW software. Second we analyze the data received by the CW radar, consequently, the Doppler frequency induced by the running fan is easily obtained through data processing. According to the characteristic of the signal in the Doppler domain, we can judge the motion of the running fan.

4.3.1 Hardware configuration of fan detection

Below is the component list of the CW radar system:

- HP E4433B ESG-D series signal generator (882MHz, 18dBm)
- ZC2PD-900 power splitter (800-900MHz)
- ZAMIQ-895D demodulator (868-895MHz)
- Two SLP-1.9+ low pass filters (DC-1.9MHz)
- Two HRN-0118 double ridged horn antennas (as transmitter and receiver)
- NI USB-6210 DAQmx
- Cables

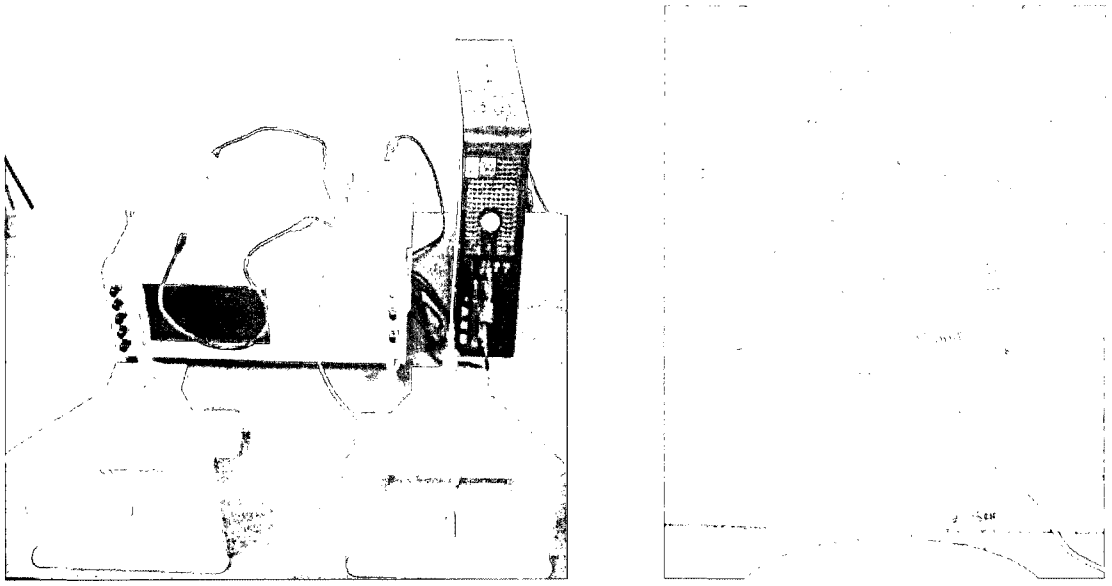

(a) The schematic of CW radar system (b) Wrapped fan behind plywood with thickness=3/4 inch

Fig4.1 The fan detection hardware system

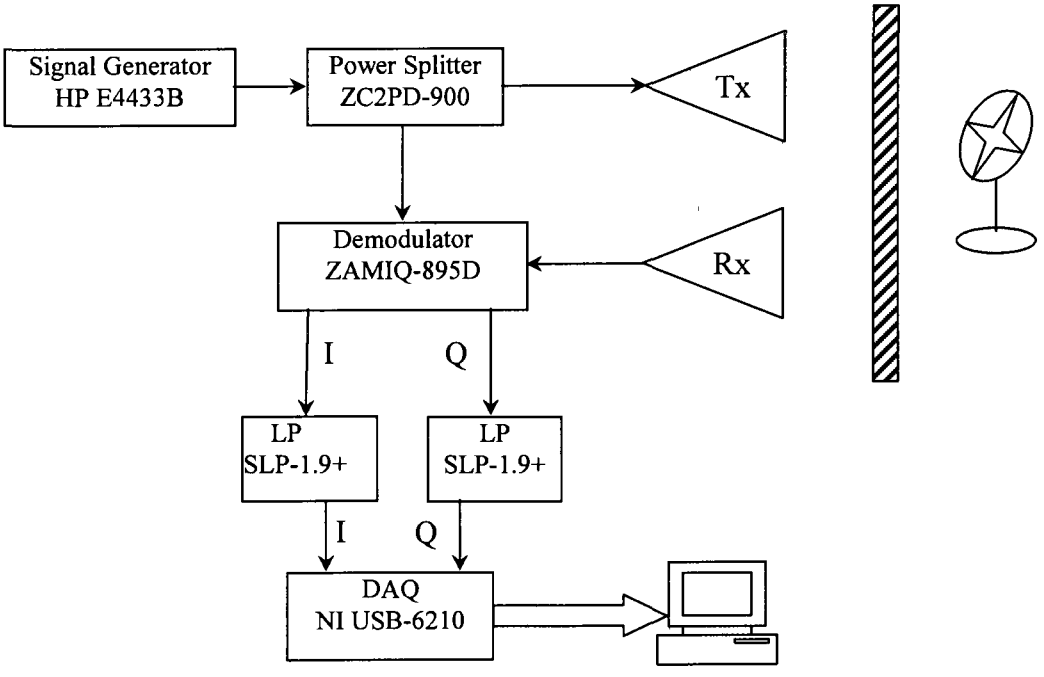

Fig4.2 The flowchart of the Doppler detection for a running fan

Fig4.1 (a) shows the hardware connection in the real application while Fig4.1 (b) shows the target–an electrical fan, which is wrapped with aluminum paper in order to get strong reflectivity. The target is separated by a 2.4m*1.2m*1.8cm plywood.

The whole hardware flowchart configuration is shown in Fig4.2. Fist we set the operating frequency and power of the signal generator to be 882MHz and 18dBm, for the sake of good penetration and maximum ratings of other instruments. Then we connect the signal generator to the power splitter, from where, one branch of the signal is sent to the transmitter antenna, and the other branch is sent to the demodulator. By the demodulator, we demodulate the signal from the receiver, then we get the IQ channel data. Next we send the IQ channel data to the NI USB-6210 data acquisition board through two low pass filters. Finally we record the data into a computer with the help of NI USB-6210.

4.3.2 Data acquisition

Different methods can be employed in the data acquisition step. We can use "Measurement & Automation Explorer", "LabVIEW SignalExpress" and "National Instruments LabVIEW 8.5.1". All of these three kinds of application software are developed by National Instrument and consistent with the NI USB-6210 data acquisition board. In this case, we made our own program by the most powerful "labVIEW" to collect the IQ data after the demodulator. After the data acquisition, we can get the time-domain IQ data at different times.

4.3.3 Time Frequency Analysis-Short Time Fourier Transform

In this part, we give the demodulated I channel data from the running fan. And analyze the Doppler domain characteristic by Short-Time Fourier Transform. STFT is a method that can provide the frequency analysis of the signal at different time. According

to the characteristic in the Doppler domain, we can judge the motion of the fan at different time.

Suppose $s(t)$ is the backscattering signal after demodulation, then the Doppler spectrogram $S(t, f_d)$ is generated by the application of STFT:

$$S(t, f_d) = \int_{t-\Delta t/2}^{+\Delta t/2} s(t') e^{-j2\pi f_d t'} dt' \tag{4.3}$$

Where, Δt is the time slice to calculate the STFT.

Actually time domain analysis and frequency domain analysis is contradiction; we can't get the high resolution in both domains simultaneously. So STFT usually divides the signal into many time sessions, and then analyze the frequency characteristic of each session to achieve the time representation. In our problem, we divided the signal into segments that last 0.5 second. Figure4.3 shows one segment of time domain waveform when t=5s after we turn off the power.

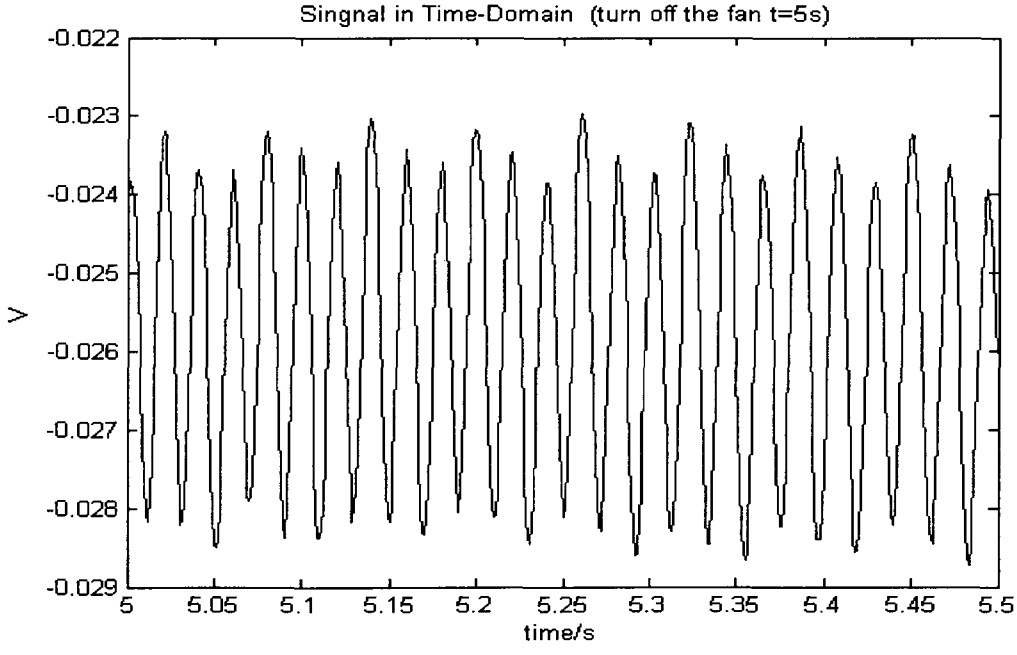

Fig4.3 The time domain signal start at t = 5-5.5s

By Short-Time Fourier Transform of the time domain data, we can get the Doppler frequency of the fan. Fig4.4 shows the signal in the Doppler domain at t=5s after we turn off the power of the fan.

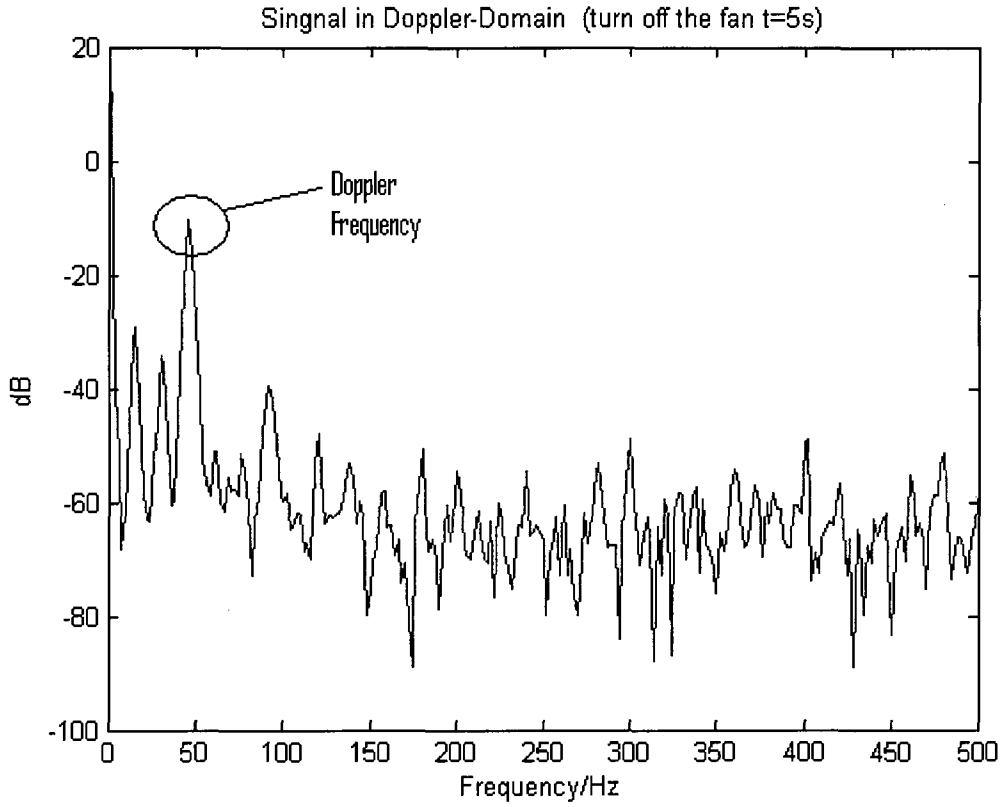

Fig4.4 The Doppler domain signal when t=5s

Fig4.5 shows the spectrogram in the time-Doppler domain. The red line in the figure gives us the whole process when we turn off the fan. In the first 4 seconds after we turn off the power, the Doppler frequency is about 50Hz, which means the velocity of the pan doesn't decrease so much. But beginning at t=5s, the Doppler frequency decrease apparently, and finally became 0Hz at t =22 s. That means the velocity of the fan keep decreasing to zero after we turn off the power. It takes 22 seconds for the fan to complete this process.

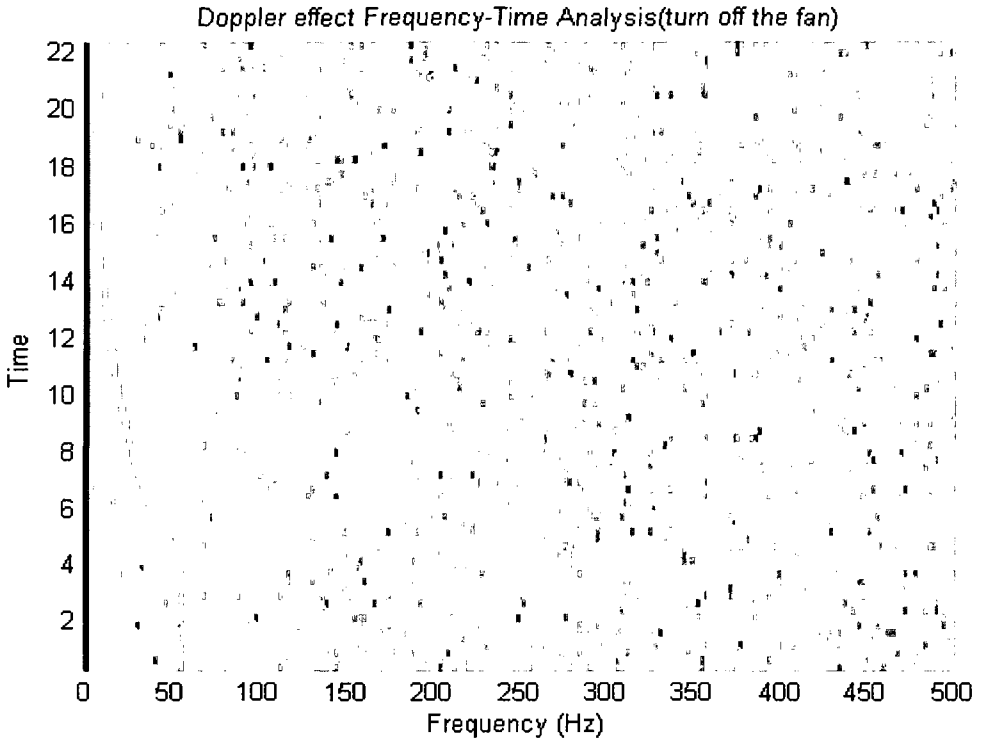

Fig4.5 The Time-Doppler domain analysis of the whole process

4.4 Micro-Doppler detection of human being movements

In this section, the CW radar is used to detect the gait of human walking. Instead of putting a running fan behind the plywood wall, a person is walking behind it. The hardware setting and the data processing are the same as detecting the running fan.

Fig4.6 shows the I Q channel signal in time domain after demodulation, which is collected directly by NI USB-6210 DAQmx. Fig4.7 is the spectrogram of the walking process as a function of Doppler frequency and time. The central red line at Doppler frequency equals zero is caused by the noise. The fluctuant curve represents the swing of the arms when people walk.

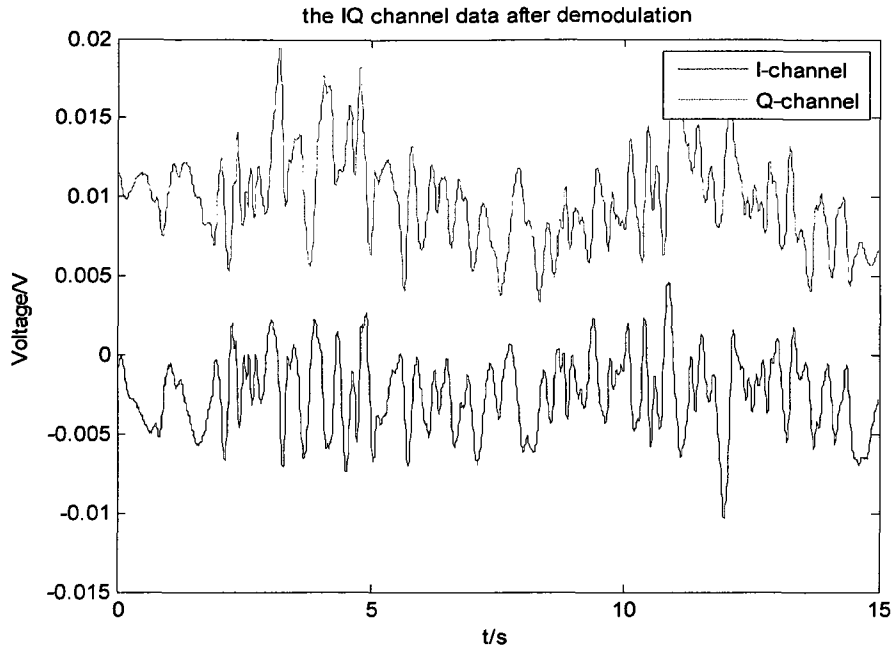

Fig4.6 The IQ channel data of human walking

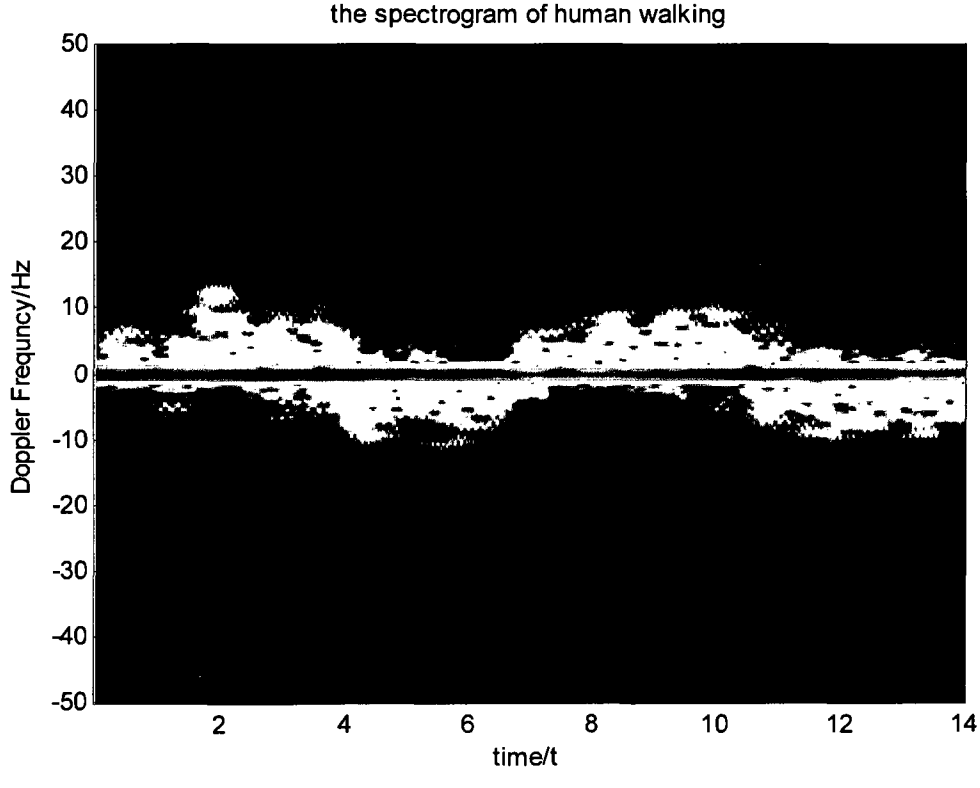

Fig4.7 The spectrogram of human walking

4.5 Azimuth detection and target track based on Doppler

In this section, we try to track the target based on resolving the Doppler frequencies and the direction of arrival (DOA) of the echoed signal from two swinging metallic corner reflectors. Fig4.8 and Fig4.9 show the schematic of the target and radar system respectively.

The concept combines the Doppler discrimination offered by the reflectors movement with the direction of arrival (DOA) information that can be collected using a small antenna array to provide the necessary information for human movement tracking. For instance, provided multiple targets are moving at different radial velocities with respect to the radar, it is possible to determine the azimuth DOA or bearing of the targets using just two antenna elements spaced in the horizontal direction. The radar configuration is shown Fig4.9.

More explicitly, if we assume the time signals received at the two antenna elements after demodulation with the carrier signal to be $r_1(t)$ and $r_2(t)$, which is shown in Fig4.10, then after the short-time Fourier transform (STFT), the spectrograms of the received signal become $R_1(f,t)$ and $R_2(f,t)$ respectively as shown in Fig4.11 and Fig4.12. If the targets of interest generate different Doppler frequencies f_i at time t due to the difference in their velocities with respect to the radar transceiver, then the DOA of the i th target with respect to the array boresight is given by equation (4.4)

$$\theta_{AZi}(t) = \sin^{-1}\left[\frac{\angle R_1(f_i,t) - \angle R_2(f_i,t)}{(2\pi d/\lambda_c)}\right] \tag{4.4}$$

where λ_c is the wavelength of the carrier, d is the space of the two horizontal receivers, to avoid phase aliasing, we chose d=0.3m in this experiment.

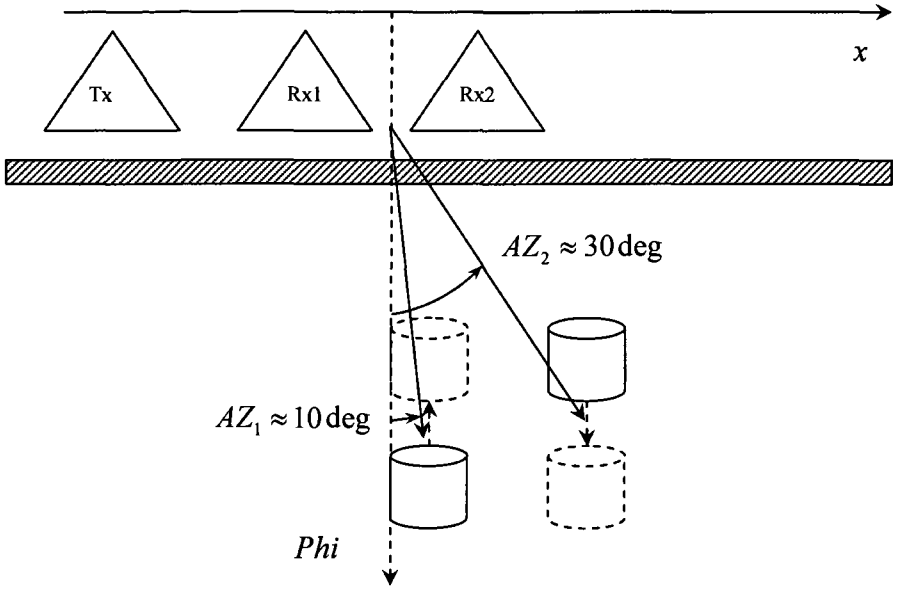

Fig4.8 The azimuth detection of two swing metallic reflectors

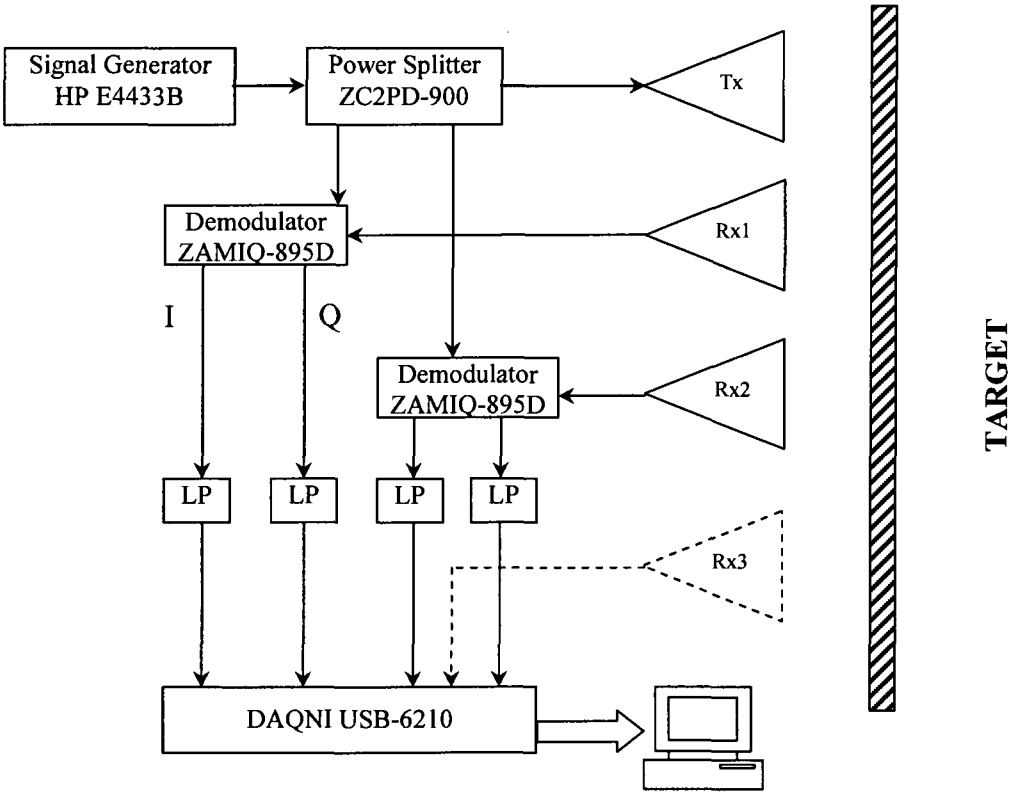

Fig4.9 The flowchart of azimuth & elevation detection

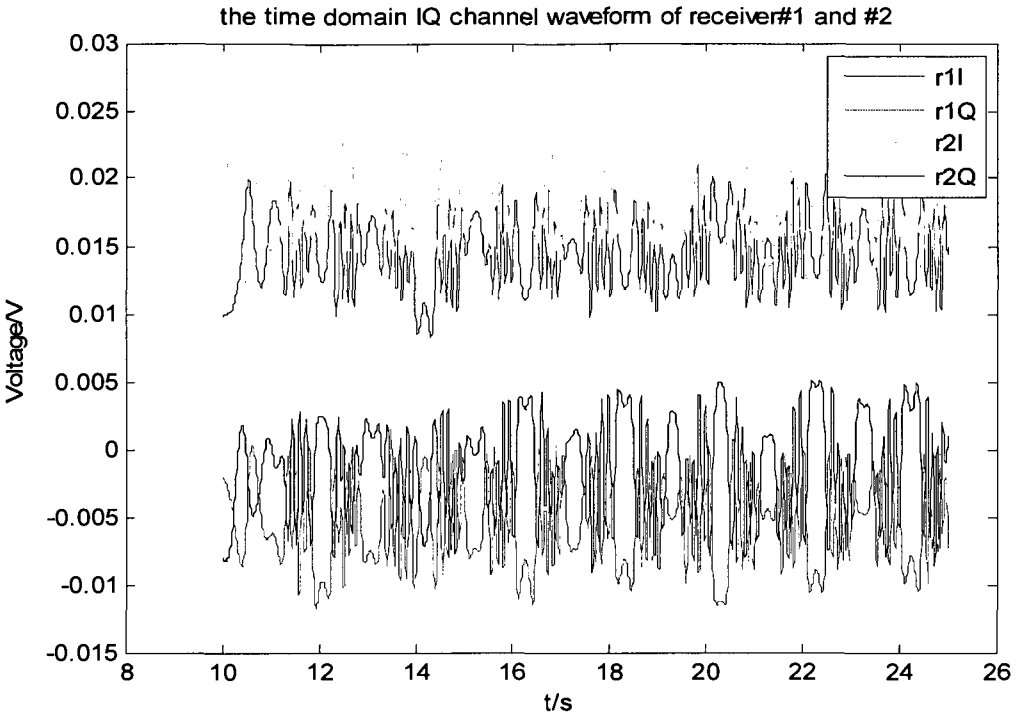

Fig4.10 The received signal in time domain after demodulation

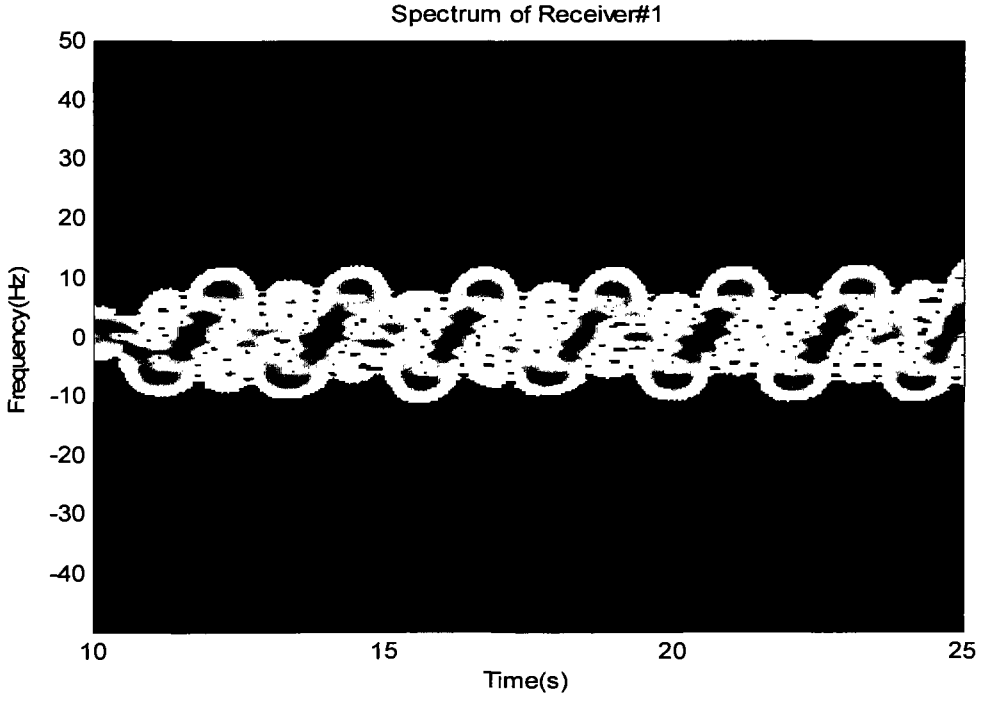

Fig4.11 The spectrogram of receiver #1

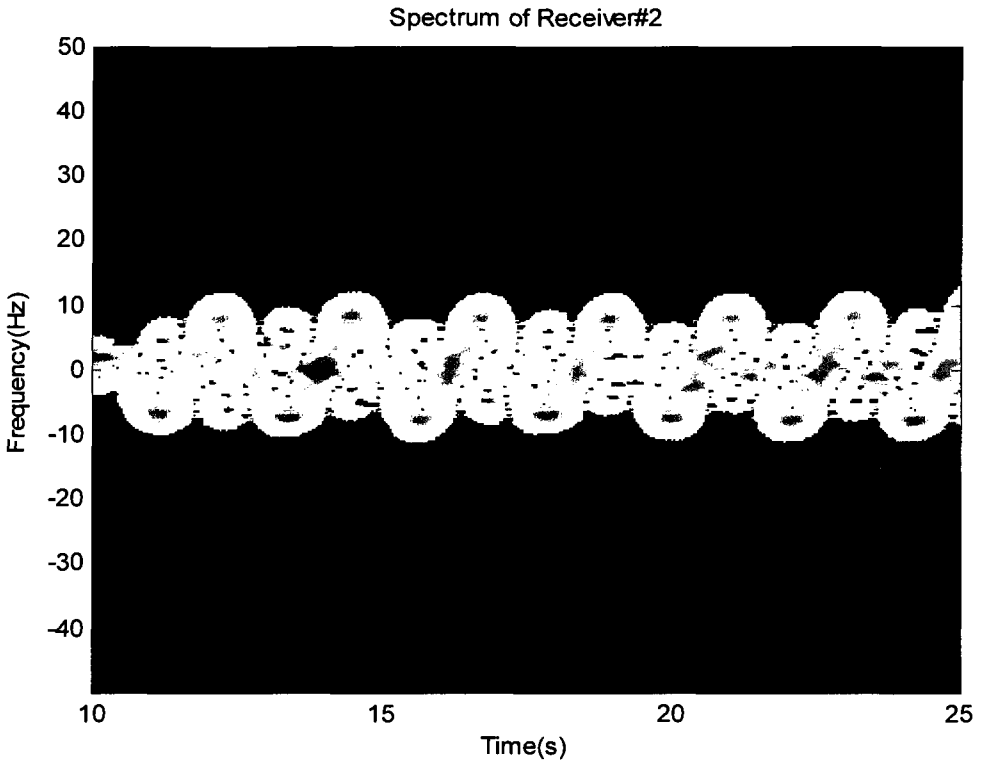

Fig4.12 The spectrogram of receiver #2

Since we can get the spectrogram of the two received signal by short-time Fourier transform (STFT), as shown in Fig4.11 and Fig4.12, we can get the azimuth information of the two swing target through equation (4.4). Fig4.13 shows the azimuth of the two reflectors as a function of Doppler and DOA.

In Fig4.13, apparently we can see two distinct sinusoidal waves, which represent the two swing metallic reflectors. Different colors means different azimuth angles in the picture according to the color bar. The yellow sinusoidal wave represents the first corner reflector with the azimuth of about 10 degree, while the red sinusoidal wave represents the second corner reflector with the azimuth of about 30 degree. This matches the targets setting in Fig4.8 very much.

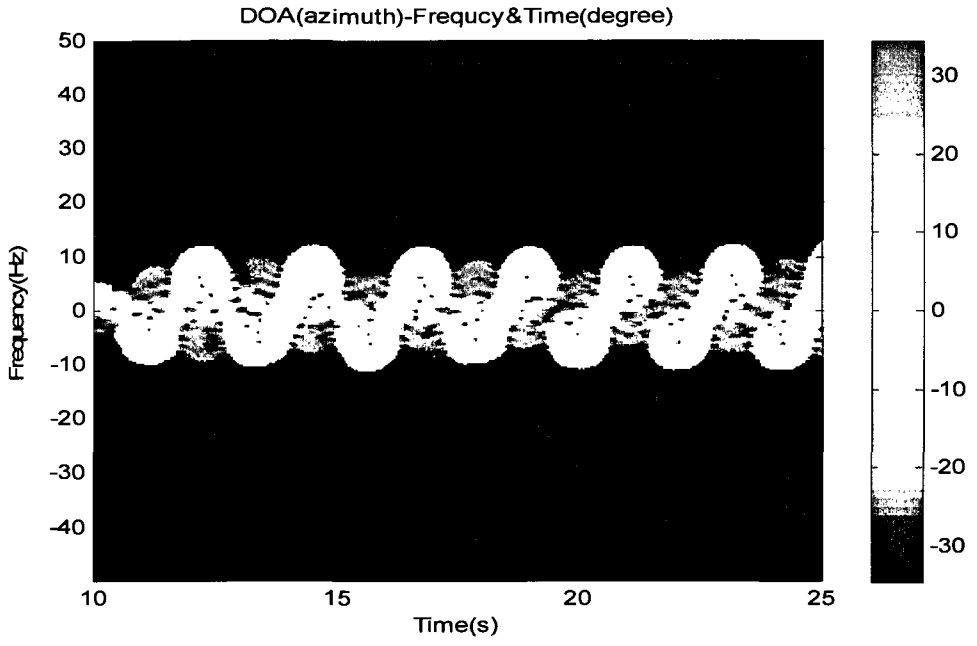

Fig4.13 The azimuth of two swing reflectors

More clearly, we can extract the azimuth information in Fig4.13, and then plot the azimuth as a function of time to track the two corner reflectors. Fig4.14 shows the trajectories of the two corner reflector as a function of time.

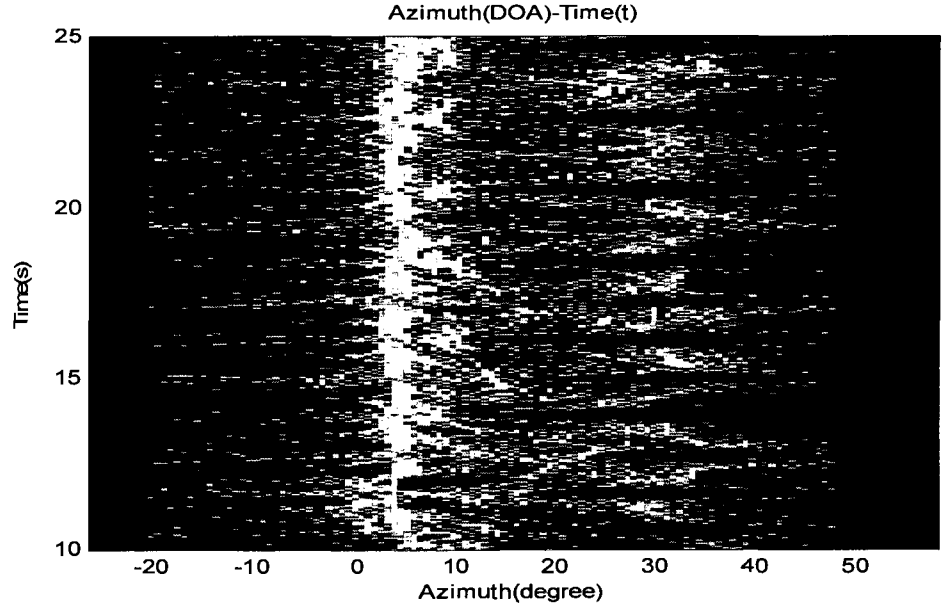

Fig4.14 The trajectory of the two swing corner

4.6 Azimuth and elevation detection based on Doppler

Since the azimuth information can be detected through a two antennas array in the horizontal direction, the elevation information of the targets can also be determined in the same way- by employing the third receiver in the vertical direction to from a vertical array. The dashed receiver in Fig4.9 shows the third antenna.

The target setting of both azimuth and elevation detection is shown in Fig4.15. A shaking corner reflector moves form the upper right corner to the lower left corner in the radar cross view.

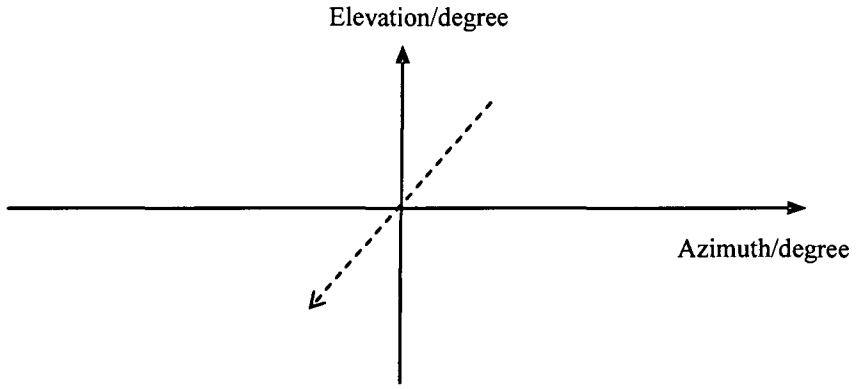

Fig4.15The schematic of the moving reflector

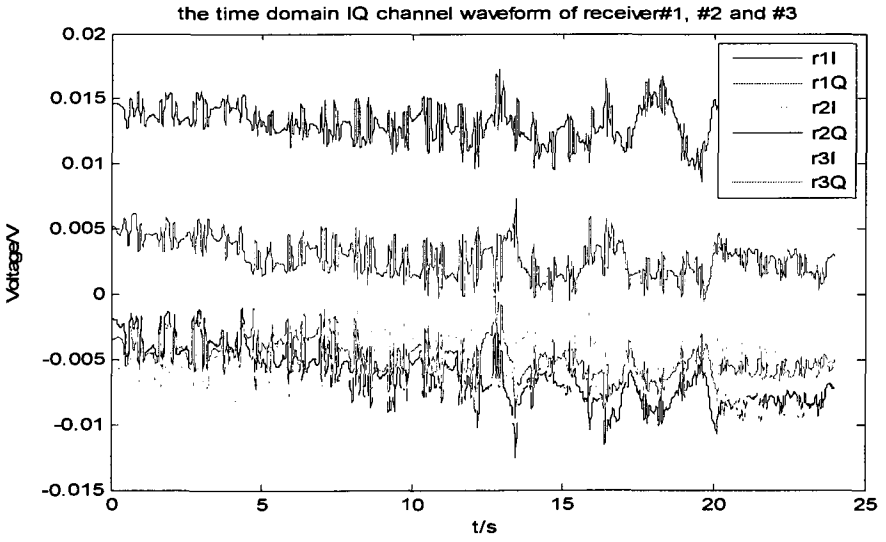

Fig4.16 The received signal in time domain after demodulation

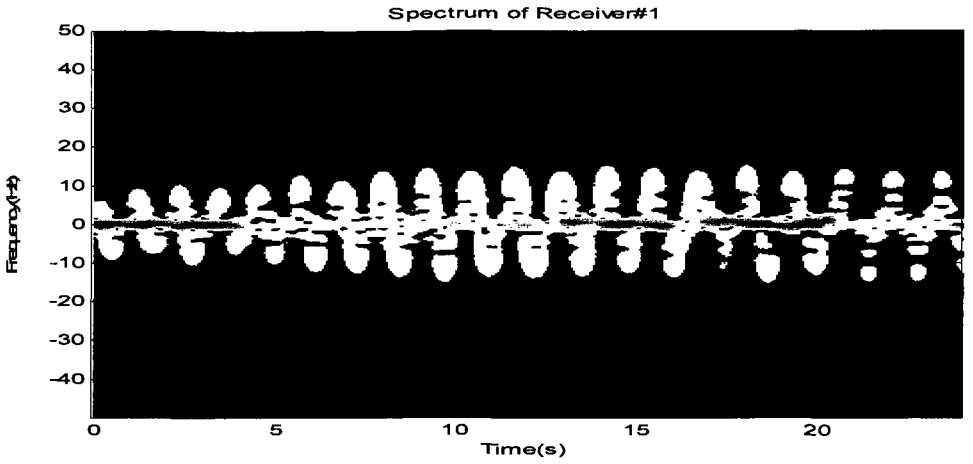

Fig4.17 The spectrogram of receiver #1 after STFT

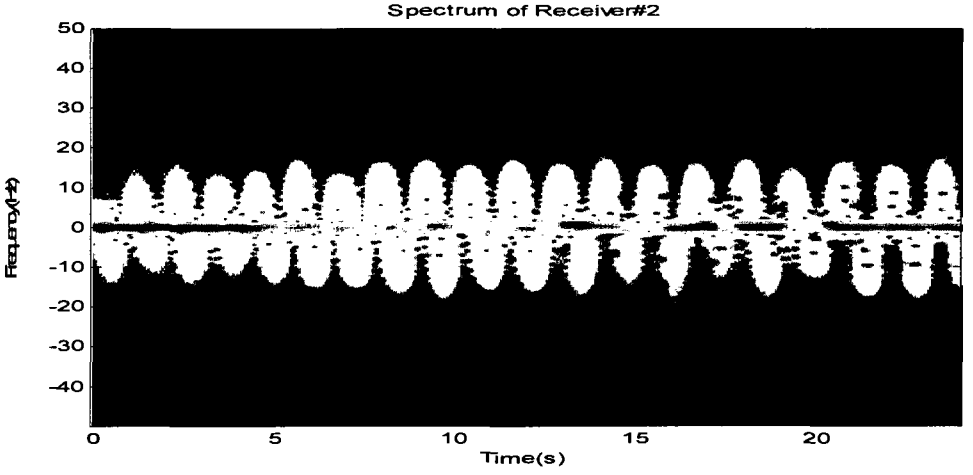

Fig4.18 The spectrogram of receiver #2 after STFT

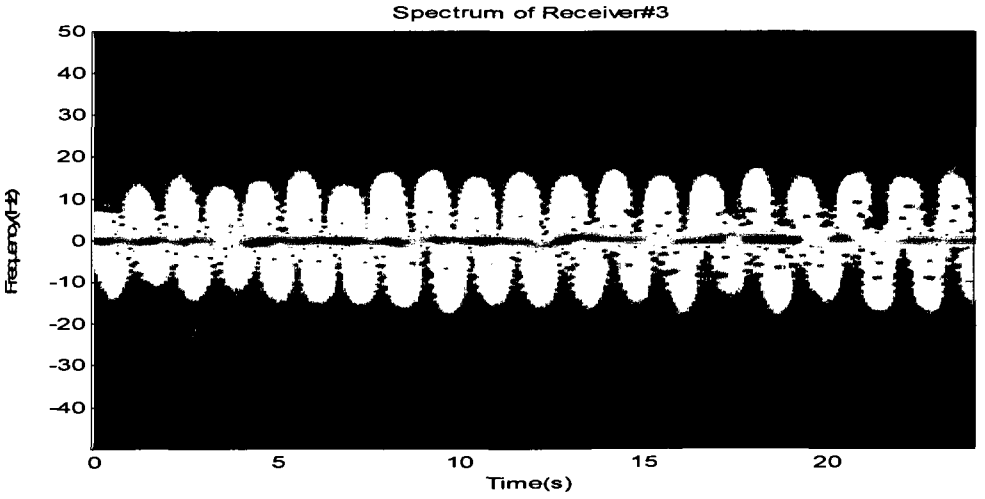

Fig4.19 The spectrogram of receiver #3 after STFT

Fig4.16 shows the received signals in time domain. By imposing the short time Fourier transform, the spectrograms of the signal received by the three receivers are shown in Fig4.17, Fig4.18 and Fig4.19 respectively. So the azimuth direction can by calculated by equation (4.4), which is shown in Fig4.20, the different colors indicate the different value of DOA.

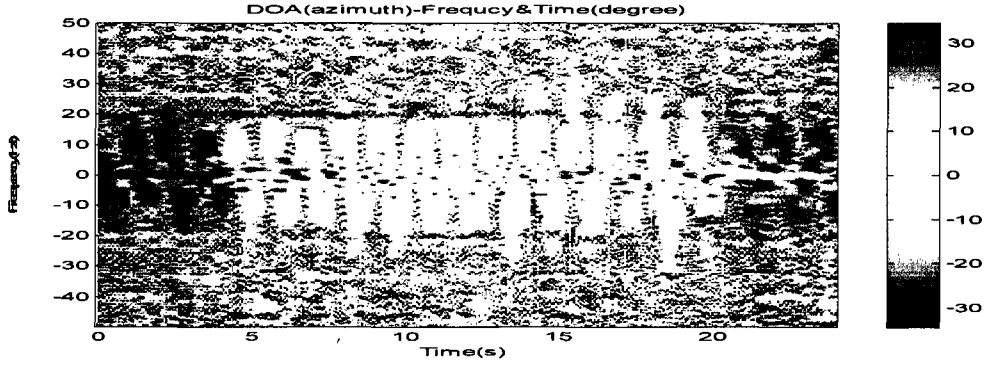

Fig4.20 The azimuth angle of the moving target in Doppler time frequency domain

The same as equation (4.4), the elevation angle can be derived as follow:

$$\theta_{ELi}(t) = \sin^{-1}\left[\frac{\angle R_1(f_i,t) - \angle R_3(f_i,t)}{(2\pi d/\lambda_c)}\right] \tag{4.5}$$

Where, $R_1(f_i,t)$ and $R_3(f_i,t)$ are the spectrogram of receiver #1 and receiver#3, which are the vertical pair of antennas. Fig4.21 shows the elevation angle as a function of time and Doppler frequency.

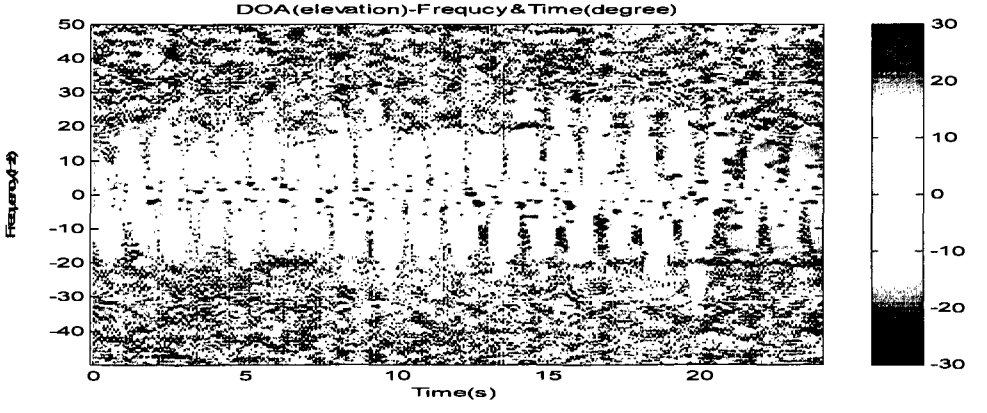

Fig4.21 The elevation angle of the moving target in Doppler time frequency domain

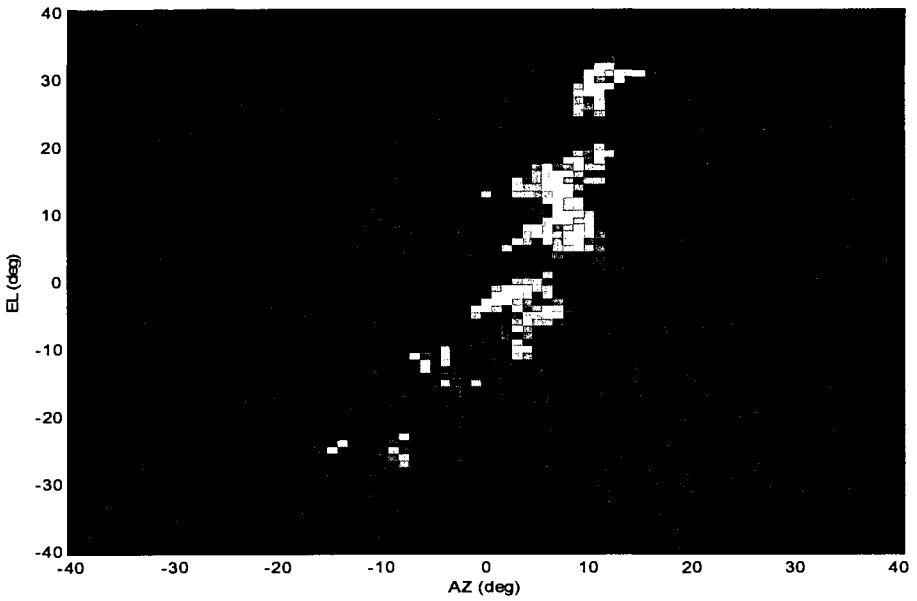

Fig4.22 The track of the target in azimuth and elevation domain

Finally the moving track of the target is shown in Fig4.22 as a function of azimuth angle and elevation angle. In this picture, it shows the target moves from upper right corner to the lower left corner and this coherent with the target setting in Fig4.15.

CHAPTER 5

CONCLUSIONS

5.1 Comparison of three through-wall radar systems

In the previous three chapters, three different through radar systems are studied. It is shown that each different radar system has its own advantages and disadvantages. In this chapter, we will compare the impulse radar, continuous wave radar and swept frequency radar in three aspects: stationary target location and imaging, micro-Doppler extraction, moving target detection and tracking.

5.1.1 Stationary location and imaging

Range resolution

The short pulse radar has a high range resolution, as we know the range resolution is $c\tau/2$, in this thesis, the duration time τ of the impulse generated by 4015D picoseconds pulse generator is about 66ps, and the range resolution is about 1cm. In the swept frequency radar system the range resolution is determined by the bandwidth of the signal. In chapter 4, the bandwidth of the swept frequency radar is 12.5GHz, so the range resolution calculated by $c/2B$ is about 1.2 cm.

Another important issue is the signal noise ratio (SNR). The low SNR ratio not only makes it difficult to detect the target from the noise, but also blurs the quality of through-wall image. Since the receiver bandwidth of impulse radar is larger enough than the

vertical network analyzer (the IF bandwidth of network analyzer is usually 10 KHz while the bandwidth of the TDS8200 receiver is usually more than 1GHz). According to the noise power formula:

$$N = kBT \tag{5.1}$$

Where, N is the noise power, k is the Boltzmann constant, $k = 1.3806505 \times 10^{-23} J/K$, T is the absolute temperature.

The CW radar usually detect moving target based on Doppler. It has a strong suppression to the stationary target; therefore, it's not good at forming a stationary imaging by CW radar.

5.1.2 Micro-Doppler extraction and moving target tracking

The micro-Doppler can be easily extracted by the CW radar system as long as the operating wavelength is small enough to induce the Doppler frequency. In our research, it is shown that the impulse radar can also detect the human breathing, but it needs higher pulse repeat rate. The maximum repeat rate of pulse generator 4015D is 500 kHz in our impulse radar system, the pulse repeat rate in Burchett's paper[2] is more than 10^6 times/second. The requirement of high pulse repeat rate will make the impulse radar system more complicated.

The moving target tracking ability of the swept frequency radar depends on the swept time of the network analyzer. In the linear swept frequency model, the swept time of network analyzer Agilent 8719ET for number of frequency (Nf) equals 201 is about 100ms. This constrains the time sampling of the moving targets.

5.1.3 Summary

Table5.1 shows the summary of the advantages and disadvantages of impulse radar, continuous wave radar and swept frequency radar in different applications.

Table5.1 Summary of the advantages and disadvantages of the three investigated radar systems

	Advantages	Disadvantages
Impulse radar	accurate range resolution and stationary target location	low SNR and require high pulse repeat rate to form image
Swept frequency radar	high imaging capacity for stationary targets	poor motion detection due to the short time required to collect coherent data from moving targets
Continuous wave radar	high SNR and micro-Doppler extraction	hard to form a stationary image

5.2 Future works

Up to present, many efforts have been done and some excellent imaging algorithms have been developed. Most of them are based on the assumption that the wall parameters are exactly known. However the wall characteristics (permittivity and depth) are unknown in practice. If the parameter of the wall is not properly considered, the through wall imaging will be distorted or even can not be achieved. So it is necessary to do more research on the microwave propagation through the wall.

In this thesis, the 2-D through wall image is given, more over, the 3-D through wall image can be got by employing more receiver array in both horizontal and vertical dimension.

REFERENCES

[1] Willie D. Jones, "No place to hide [radar devices]", IEEE Spectrum, Volume 42, Issue 11, pp.20 – 21, Nov. 2005

[2] Hugh Burchett, "Advances in Through Wall Radar for Search, Rescue and Security Application", Crime and Security, pp.511-525, June. 2006

[3] Lawrence Frazier, "MDR for Law Enforcement", IEEE Potentials, Vol.16, No.5, pp.23-26, 1998

[4] Shobha Sundar Ram, Yang Li, Adrian Lin, Hao Ling, "Doppler-based detection and tracking of humans in indoor environments", Journal of Franklin Institute, April 2008

[5] Sikl, R., Dvorak, D., Mrkvica, J., Jerabek, J., "Comparison of Pulse and Continuous Wave Propagation through the Wall", Radioelektronika, 17th International Conference, pp.1-4, April 2007

[6] W.A.van Cappellen, R.V. de Jongh, "Potentials of Ultra-Short-Pulse Time-Domain Scattering Measurements", IEEE Antennas and Propagation Magazine, Vol.42, No.4 August 2000

[7] Ram M. Narayanan, "Through-wall radar imaging using UWB noise waveforms," Journal of the Franklin Institute 345, pp.659–678, 2008

[8] T. Thayaparana, L. Stankovic, I. Djurovic, "Micro-Doppler-based target detection and feature extraction in indoor and outdoor environments," Journal of the Franklin Institute 345, pp.700–722, 2008

[9] J. Li and H. Ling, "3D ISAR image reconstruction with pose data using adaptive feature extraction", Journal of Electromagnetic Waves and Applications, vol. 15, no. 11, pp. 1571-1587, Nov. 2001.

[10] Lin Ma, Zhongzhao Zhang, Xuezhi Tan, "A Novel Through-Wall Imaging Method Using Ultra WideBand Pulse System", Intelligent Information Hiding and Multimedia Signal Processing, IIH-MSP 06 International Conference, pp.147-150, Dec. 2006

[11] Wenji Zhang, Lianlin Li, Fang Li, "Autofocusing Imaging through the Unknown Building Walls", Microwave Conference, 2008. APMC 2008, Asia-Pacific, pp.1-5, Dec.2008

[12] Aftanas, M., Rovnakova, J., Drutarovsky, M., Kocur, D., "Efficient Method of TOA Estimation for Through Wall Imaging by UWB Radar", IEEE International Conference on Ultra-Wideband, pp. 101-104, Sept.2008

[13] Maaref, N., Millot, P., Ferrieres, X., Pichot, C., Picon, O., "Experimental Through-The –Wall Detection in Cluttered Environment Using Time Reversal Processing", IEEE, Antennas and Propagation Society International Symposium, pp. 1-4, July.2008

[14 Dehmollaian, M., Sarabandi, K., "Hybrid FDTD and Ray Optics Approximation for Simulation of Through-Wall Microwave Imaging", IEEE, Antennas and Propagation Society International Symposium, pp.249-252, July.2006

[15] Hunt, A.R., "Image Formation Through Walls Using a Distributed Radar Sensor Array", Applied Imagery Pattern Recognition Workshop, Proceedings. 32nd, pp.232-237, Oct. 2003

[16] Rovnakova, J., Svecova, M., Kocur, D., Trung Thanh Nguyen; Sachs, J., "Signal Processing for Through Wall Moving Target Tracking by M-sequence UWB Radar", Radioelektronika International Conference, pp.1-4, April. 2008

[17] Dehmollaian, M., Sarabandi, K., "Simulation of Through-Wall Microwave Imaging: Forward and Inverse Models", IEEE, Geoscience and Remote Sensing Symposium, pp.407 – 410, Aug.2006

[18] Ahmad, F., Yimin Zhang, "Three-Dimensional Wideband Beamforming for Imaging Through a Single Wall", IEEE, Geoscience and Remote Sensing Letters, Volume 5, issue 2, pp.176-179, April. 2008

[19] Lubecke, V.M., Boric-Lubecke, O., Host-Madsen, A., Fathy, A.E., "Through-the-Wall Radar Life Detection and Monitoring", IEEE/MTT-S International Microwave Symposium, pp.769-772, June. 2007

[20] Cermak, D., Pidanic, J., Schejbal, V., "Through-wall propagation measurements", Radioelektronika, pp.1-4, April 2007

[21] Bugaev, A.S., Chapursky, V.V., "Through wall sensing of human breathing and heart beating by monochromatic radar", Ground Penetrating Radar, Volume 1, pp.291 – 294, 2004

[22] Ram,S.S., Ling, H., "Through-wall tracking of human moves using joint Doppler and array processing", IEEE, Geoscience and Remote Sensing letters, Volume5, issue 3, pp.537-541, July 2008

[23] Nemec, Zdenek, Mrkvica, Jan, "UWB through-wall propagation measurements", Antennas and Propagation, EuCAP, pp.1-6, Nov.2006

[24] "Through wall imaging of the objects scanned by M-sequence UWB radar system", Radioelektronika 18th International Conference, pp.1-4. April.2008

APPENDIX

Matlab Codes

****

1. Matlab Code for 1-D range profile

```
clear;
clc;

% target settings
Ns=51;                                  % the discretization number
x=linspace(-5,5,Ns)';                    % the target range -5m  to 5m
sigma=linspace(0,100,Ns)';
figure(1);
plot(x,sigma,'*'); title('the target model'); xlabel('x/m');
ylabel('sigma');
axis([-10 10 0 110]);


% frequency settings
c=3.0e8;
f1=1e9;
f2=5e9;
Nf=401;
f=linspace(f1,f2,Nf);
dr=c/(2*(f2-f1));

% data collection
R0=10000;                                % the radar is at a distance of
r=R0+x;
Es=sigma*ones(1,Nf).*exp(-j*4*pi/c*r*f);
Es=sum(Es);
figure(2);
plot(f,abs(Es)); axis tight;
xlabel('f/Hz'); title('the amplitude of the echo signal in frequency
domain');

% range compensation
Esc=Es.*exp(j*4*pi*f/c*R0);

Escw=Esc.*hamming(Nf).';

% calculate the range profile
figure(25);
plot(abs(fftshift(ifft(Es))));
xlabel('x/m');title('range profile');
```

```
figure(3);
plot(dr*(-(Nf-1)/2:(Nf-1)/2),abs(fftshift(ifft(Esc))));
xlabel('x/m');title('range profile');

figure(4);
plot(dr*(-(Nf-1)/2:(Nf-1)/2),abs(fftshift(ifft(Escw))));
xlabel('x/m');
title('range profile after the hamming window function');
```

2. Moving Target Detection by Merge Power splitter

```
clear;
clc;
%%% 201, swept time:   100ms
%%% 401,               200ms
%%% 801,               400ms

%target setting
x1=0.46;                % the position of receiver1
x2=-0.46;               % the position of receiver2
xt=0;                   % the position of transmitter

f1=1.0*10^9;
f2=13.5*10^9;
Nf=401;
f=linspace(f1,f2,Nf);
c=3.0*10^8;
dr=c/(f2-f1);
r=(0:Nf-1)*dr;

time=load('C:\study\thesis\hui\merge receiver
measurements\VNA\401\time.lvm');
t_scan=(time-time(4))/1000;
N=length(t_scan);
t_scan=t_scan(4:N);

figure(1);
plot(t_scan); title('time consuming to collect the data');
xlabel('number of scan'); ylabel('time/s');

background=load('C:\study\thesis\hui\merge receiver
measurements\VNA\401\background.txt');
background=background(:,1)+i*background(:,2);
background=reshape(background,Nf,[]);
r_back=fftshift(ifft(background));
r_back=abs(r_back);

figure(2);
plot(r,r_back(:,6));title('the range profile of the background');
xlabel('Range/m');


data=load('C:\study\thesis\hui\merge receiver
```

```
measurements\VNA\401\data.txt');
data=data(:,1)+i*data(:,2);
data=reshape(data,Nf,[]);
data=data-background(:,4)*ones(1,N);
data=data(:,4:N);
r_reflector=fftshift(ifft(data));
r_reflector=abs(r_reflector);
N=N-3;

figure(3);
imagesc(t_scan,r,r_reflector);  axis xy; title('the total range profile
after background subtraction');
xlabel('t/s'); ylabel('distance/m');
figure(4);
plot(r,r_reflector(:,3)); title('the range profile of corner reflector
at certain position'); %axis([min(r) max(r) 0 0.03]);
xlabel('Range/m');

r1=[5.52,5.952,5.952,6.192,6.384,6.648,6.864,7.224]-3.5;
intensity1=[0.001709,0.002728,0.006136,0.005962,0.007607,0.005178,0.003
858,0.004332];
r2=[7.128,7.488,7.728,8.088,8.256,8.664,8.832,9.192]-5.2;
intensity2=[0.005986,0.004188,0.003156,0.0022,0.002185,0.0009515,0.0010
66,0.0006604];

figure(45);
plot(r2);

%% imaging domain
Ixmax=2;                                          % image domain
1.5m*1.5M
Iymax=3;
ix=-Ixmax/2:dr/2:Ixmax/2;
iy=0:dr:Iymax;
[Ix,Iy]=meshgrid(ix,iy);
Nix=length(ix);
Niy=length(iy);
Ni=Nix*Niy;                                     % number of imaging
pixels
Image=zeros(Niy,Nix);



for kx=1:Niy
    for ky=1:Nix
        dt=Ix(kx,ky).^2+Iy(kx,ky).^2;
        dt=sqrt(dt);
        d1=(Ix(kx,ky)-x1).^2+(Iy(kx,ky)-0).^2;
        d1=sqrt(d1);
        d1=d1+dt;

        d2=(Ix(kx,ky)-x2).^2+(Iy(kx,ky)-0).^2;
        d2=sqrt(d2);
        d2=d2+dt;
        if(abs(d1-r1(8))<=dr) %&&&abs(d2-r2(1))<=dr
```

```
            Image(kx,ky)=intensity1(8);%+intensity2(1);
        end
        if(abs(d2-r2(8))<=dr)
           Image(kx,ky)=intensity2(8)+Image(kx,ky);
        end
    end
end

figure(5);
imagesc(ix,iy,Image); axis xy;
title('the radar image of the two reflectors');
xlabel('x/m'); ylabel('y/m');
```

BIOGRAPHICAL SKETCH

Xiaohui Wang was born in P.R.China in Dec.1981 as the son of Jingzhang Wang and Ronguo Wu. He received his bachelor, Master's Degree in Electrical Engineering of Northwestern Polytechnical University, Xi'an, Shaanxi, P.R.China in 2004 and 2007 respectively. His master research in China was focus on the RCS measurement and radar imaging. In June, 2007, he joined Master program in Electrical Engineering department of the University of Texas-Pan American. His research fields include through wall radar imaging, electromagnetic computation, automatic control, antenna measurement and design.